NASA TECHNICAL MEMORANDUM

STATIC LONGITUDINAL CHARACTERISTICS OF A MISSILE CONFIGURATION OF FINENESS RATIO 14.7 FROM MACH 0.30 TO 0.93

by Edward J. Ray

Langley Research Center
Langley Station, Hampton, Va.

NATIONAL AERONAUTICS AND SPACE ADMINISTRATION - WASHINGTON, D. C. - NOVEMBER 1965

60

NASA TM X-1175

STATIC LONGITUDINAL CHARACTERISTICS OF A MISSILE CONFIGURATION OF FINENESS RATIO 14.7 FROM MACH 0.30 TO 0.93

By Edward J. Ray

Langley Research Center
Langley Station, Hampton, Va.

NATIONAL AERONAUTICS AND SPACE ADMINISTRATION

STATIC LONGITUDINAL CHARACTERISTICS OF A MISSILE CONFIGURATION OF FINENESS RATIO 14.7 FROM MACH 0.30 TO 0.93*

By Edward J. Ray
Langley Research Center

SUMMARY

10304

The static longitudindal aerodynamic characteristics of a missile configuration of fineness ratio 14.7 combined with five different aft-fin arrangements have been determined in a wind tunnel throughout a Mach number range from 0.30 to 0.93 corresponding to a range of Reynolds numbers per foot (per 30.5 cm) from 1.80×10^6 to 3.62×10^6. Three of the configurations were tested in a roll attitude of 45°. The roll effectiveness for two of the body-fin combinations was determined over the Mach range at several angles of attack.

The investigation indicated that the body combined with the various aft-fin arrangements exhibited essentially linear variations of lift coefficient and pitching-moment coefficient at small angles of attack throughout the test Mach number range. Tests of three of the fin-body configurations indicated that static longitudinal stability and lift-curve slopes would be reduced when the configurations were rolled to 45°. Roll effectiveness was evident for two of the body-fin combinations at 0° and 5° angles of attack; however, increases in angle of attack from 5° to 10° resulted in large reductions in the increase of roll effectiveness with angle of attack.

INTRODUCTION

An investigation has been made in a wind tunnel at Mach numbers from 0.30 to 0.93 to determine the static longitudinal aerodynamic characteristics of a missile configuration having a fineness ratio of 14.7 and an ogive-shaped nose with a cylindrical afterbody equipped with various fin arrangements.

This paper presents the normal force, lift, drag, and pitching-moment results obtained for the body alone and the body combined with five different fin configurations. The fins were positioned near the base of the body with one set of vertical fins and one set of horizontal fins. Also presented are the longitudinal data for the body with three

different fin arrangements rolled to 45°. In addition, the data presented include the roll-effectiveness parameters determined for the body combined with two different fin configurations at several angles of attack throughout the Mach number range.

The average test Reynolds number per foot (per 30.5 cm) varied from 1.80×10^6 to 3.62×10^6 and the angle-of-attack range generally extended from -4° to 10°.

SYMBOLS

The data are referred to the wind-axis system except for the normal-force coefficients and lateral data which are referred to the body-axis system. The moment-reference point is on the fuselage center line at a longitudinal position 32.33 inches (82.12 cm) aft of the model nose apex. (See fig. 1(a).) A reference area of 0.06345 square foot (0.006 m^2) and a reference span and chord of 1.80 inches (4.57 cm) were used to nondimensionalize the data.

Measurements for this investigation were taken in the U.S. Customary System of Units. Equivalent values are indicated herein parenthetically in the International System (SI) in the interest of promoting use of this system in future NASA reports. Details concerning the use of SI, together with physical constants and conversion factors, are given in reference 1.

b	reference span, 1.80 in. (4.57 cm)
C_D	drag coefficient, $\frac{\text{Drag}}{qS}$
C_{D_o}	drag coefficient at zero lift
C_L	lift coefficient, $\frac{\text{Lift}}{qS}$
C_l	rolling-moment coefficient, $\frac{\text{Rolling moment}}{qSb}$
C_m	pitching-moment coefficient, $\frac{\text{Pitching moment}}{qS\bar{c}}$
C_N	normal-force coefficient, $\frac{\text{Normal force}}{qS}$
C_{L_α}	lift-curve slope, $\frac{\partial C_L}{\partial \alpha}$, per deg (near $\alpha = 0^\circ$)
C_{m_α}	pitch-curve slope, $\frac{\partial C_m}{\partial \alpha}$, per deg (near $\alpha = 0^\circ$)
C_{l_δ}	rolling-moment effectiveness parameter, $\frac{\partial C_l}{\partial \delta}$ (near $\alpha = 0^\circ$)

$\frac{\partial C_m}{\partial C_N}$	longitudinal stability parameter (near $\alpha = 0^o$)
c	local chord, in. (cm)
$\bar{c}$	reference chord, 1.80 in. (4.57 cm)
l	body length, 50.56 in. (128.42 cm)
M	Mach number
q	free-stream dynamic pressure, lb/sq ft (N/m^2)
R	Reynolds number
S	reference area, 0.06345 sq ft (0.006 m^2)
t	thickness, in. (cm)
x	distance from nose apex along body axis, in. (cm)
α	angle of attack, deg
δ	angle of fin deflection (positive for negative rolling moments), deg
ϕ	angle of fin roll (zero with one set of fins vertical and one set horizontal), deg

MODELS

A two-view drawing of the body combined with the fin 1 arrangement is shown in figure 1(a). As shown in this figure, the body of the configuration incorporated an ogival nose and a boattailed afterbody. A rearward-facing step was located at model station 26.54 inches (67.41 cm) for the purpose of increasing the boundary-layer thickness. The diameters at various stations along the body axis and other pertinent geometric characteristics of the body are presented in table I.

The various fin planforms which were tested with the body are shown in figure 1(b). All the fin arrangements had identical spans, trailing-edge locations on the body, and chord lengths at the body juncture. The leading-edge sweep of fins 1 and 2 was 60^o and the leading-edge sweep of fins 3, 4, and 5 was 45^o. A double-wedge airfoil section was employed for all the fin configurations. The thickness ratios of the airfoils and other geometric details of the fins are listed in table I. Photographs of the complete model with the fin 1 arrangement are presented in figure 2.

TEST AND CORRECTIONS

The investigation was made in the Langley high-speed 7- by 10-foot tunnel with the slots in the test section closed. Test Mach numbers, dynamic pressures, and average test Reynolds numbers per foot (per 30.5 cm) for this investigation are shown in the following table:

M	q		R per ft (per 30.5 cm)
	lb/ft^2	N/m^2	
0.30	129	6 177	1.80×10^6
.40	215	10 294	2.33
.60	421	20 157	3.10
.70	528	25 281	3.40
.81	630	30 164	3.60
.86	678	32 463	3.60
.93	731	35 000	3.62

The configuration was sting mounted and forces and moments were measured with an internally mounted six-component strain-gage balance through an angle-of-attack range from about -4° to 10°. Tests were conducted through the Mach range with the body alone and with the body combined with five different fin configurations. Each of the five fin arrangements consisted of four fins, with one set of fins positioned vertically and the other set positioned horizontally. Three of the body-fin combinations were tested at a roll angle of 45° to determine the effect of roll angle on the longitudinal characteristics. In addition, roll effectiveness parameters for two of the body-fin combinations were determined throughout the Mach number and angle-of-attack ranges by deflecting each fin 1°.

Transition strips approximately 1/8 inch (0.32 cm) wide of No. 120 carborundum grains were placed 1 inch (2.54 cm) from the nose apex and at the 5-percent-chord station of the tail fins to assure a turbulent boundary layer at the lowest test Mach number. The angles of attack have been corrected for deflection of the sting-support system and balance combination due to aerodynamic loads. Base-pressure measurements were obtained by use of a static-pressure tube located inside of the model base and the data were corrected to correspond to a pressure at the base equal to free-stream static pressure. Jet-boundary and blockage corrections calculated by the methods of references 2 and 3, respectively, have been applied to the data.

PRESENTATION OF DATA

The results of the investigation at Mach numbers ranging from 0.30 to 0.93 are presented in the following figures:

DISCUSSION OF RESULTS

Longitudinal Characteristics

Effect of fin configuration on longitudinal characteristics.- The variations of the lift and normal-force coefficients with angle of attack at Mach numbers ranging from 0.30 to 0.93 for the body alone and for the body combined with five different fin arrangements are shown in figures 3 and 4, respectively. In general, as compared with the body-alone configuration, all the body-fin combinations exhibited substantial increases in lift-curve

slope and essentially linear variations of lift coefficient with angle of attack in the low angle-of-attack range. It will be noted that the variation of lift coefficient became increasingly nonlinear with increasing angle of attack for all body-fin combinations as a result of the component of flow across the inclined cylinder. (See ref. 4.) A summary of the variations of the lift-curve slopes, near zero lift, with Mach number for the various test configurations is presented in figure 7. These results show that the lift-curve slopes for the body-alone configuration were small compared with those for the body-fin combinations and remained essentially constant throughout the test Mach number range. The body-fin combinations generally indicated a slight increase in lift-curve slope with increasing Mach number up to a Mach number of about 0.85. Since all these data were nondimensionalized by using the same reference area, the body combined with the largest of the fins, the trapezoidal fin 3, exhibited the highest lift-curve slopes.

Figure 5 presents the variations of pitching-moment coefficient with angle of attack for the test configurations at Mach numbers from 0.30 to 0.93. The pitching-moment results for the body-alone configuration (fig. 5(a)) indicate essentially linear variations of pitching-moment coefficient with angle of attack in the lower angle-of-attack range. As would be expected, with the chosen moment reference, the body of revolution was highly unstable. Addition of the aft fins resulted in stable pitching-moment variations with angle of attack for all the body-fin combinations. (See figs. 5(b) to 5(f).) A summary of the pitch-curve slopes C_{m_α} for the various test configurations over the Mach number range is shown in figure 7. These results show that the instability of the body alone, as indicated by the positive values of C_{m_α}, was constant over the entire Mach number range. The pitch-curve slopes for the body-fin combinations indicated a gradual increase in longitudinal stability up to a Mach number of about 0.80. Longitudinal stability decreased slightly for all the body-fin combinations for Mach numbers greater than about 0.80.

The aerodynamic-center locations at the various test Mach numbers for the body-alone and body-fin configurations are shown in figure 8. The aerodynamic-center locations in fraction of body length from the nose apex were determined from the basic data in figures 4 and 5. The values were calculated using the equation

$$\text{a.c.} = \frac{x_{(\text{moment ref.})}}{l} - \frac{\dfrac{\partial C_m}{\partial \alpha}}{\dfrac{\partial C_N}{\partial \alpha}} \times \frac{\bar{c}}{l} \tag{1}$$

Because of the small reference coefficients used in the reduction of the data and the resulting nonlinearities in the data points, it was difficult to determine the slope of the curves in the low angle-of-attack range accurately. Significant trends, however, were established in the aerodynamic-center locations for the test configurations. As shown in

figure 8(a), the aerodynamic-center location for the body-alone configuration was about 0.051 body lengths behind the nose apex for Mach numbers ranging from 0.30 to 0.70. Because of the abrupt divergence of the boattailed afterbody, separation of flow may have contributed to the extreme forward location of the aerodynamic center for the body-alone configuration. As shown in figure 8, the addition of the aft fins to the body resulted in large rearward shifts in the aerodynamic-center locations on the configurations. The variations of aerodynamic-center location with Mach number for the body combined with the various fin arrangements were small throughout the test Mach number range.

Effect of roll angle on the longitudinal characteristics of the configuration.- The basic data indicating the longitudinal characteristics of body-fin 1 configuration, the body-fin 3 configuration, and the body-fin 5 configuration rolled to 45° are included in figures 9 to 11. The summary data of figures 12(a) to 12(c) indicate that the effects of roll angle on the longitudinal characteristics of the three configurations tested in this attitude were similar. The lift-curve slopes C_{L_α} and longitudinal stability, as indicated by pitch-curve slopes C_{m_α} decreased for the three test configurations in the rolled position. This reduction in lift-curve slope and longitudinal stability is presumed to be due to unfavorable interference (blanketing effect) of the lower set of fins on the upper set of fins. As expected, the drag values at zero lift C_{D_0} remained essentially the same for each of the three configurations in the unrolled or rolled positions since there were no changes in the wetted areas.

Roll Effectiveness

The variations of roll-effectiveness parameters C_{l_δ} with Mach number for the body combined with fin 1 and the body combined with fin 3 are shown in figure 13. The body combined with the larger of the two fin arrangements, fin 3, was about 23 percent more effective in roll than the body combined with fin 1 at an angle of attack of 0°. An increase in angle of attack from 0° to 5° resulted in increases in roll effectiveness for both of the test configurations; however, the increase in roll effectiveness for the body-fin 1 configuration was less than for the body-fin 3 configuration. At Mach numbers ranging from 0.30 to 0.80, the roll effectiveness of the body-fin 1 configuration at a 10° angle of attack was about the same as the roll effectiveness at a 5° angle of attack. At Mach numbers higher than 0.80, the roll effectiveness at a 10° angle of attack for the body-fin 1 configuration fell below the values for the configuration at a 5° angle of attack. The increase in roll effectiveness for the body with fin 3 from a 5° to 10° angle of attack was about 50 percent less than the increase from a 0° to 5° angle of attack.

CONCLUDING REMARKS

The results of a wind-tunnel investigation made to determine the static longitudinal characteristics of a missile configuration of fineness ratio 14.7 equipped with various aft-fin arrangements indicated the following conclusions:

1. The body combined with five different aft-fin arrangements, each varying in planform, exhibited essentially linear variations of lift coefficient and pitching-moment coefficient at small angles of attack throughout the Mach range of 0.30 to 0.93.

2. Tests of the body combined with three different fin arrangements indicated that the static longitudinal stability and the lift-curve slope would be reduced when the configurations were rolled to 45°.

3. Roll effectiveness was evident for two of the body-fin configurations at 0° and 5° angles of attack. Increases in angle of attack from 5° to 10°, however, resulted in large reductions in the increase of roll effectiveness with angle of attack.

Langley Research Center,
National Aeronautics and Space Administration,
Langley Station, Hampton, Va., August 16, 1965.

REFERENCES

1. Mechtly, E. A.: The International System of Units - Physical Constants and Conversion Factors. NASA SP-7012, 1964.

2. Gillis, Clarence L.; Polhamus, Edward C.; and Gray, Joseph L., Jr.: Charts for Determining Jet-Boundary Corrections for Complete Models in 7- by 10-foot Closed Rectangular Wind Tunnels. NACA WR L-123, 1945. (Formerly NACA ARR L5G31.)

3. Herriot, John G.: Blockage Corrections for Three-Dimensional-Flow Closed-Throat Wind Tunnels, With Consideration of the Effect of Compressibility. NACA Rept. 995, 1950. (Supersedes NACA RM A7B28.)

4. Allen, H. Julian; and Perkins, Edward W.: Characteristics of Flow Over Inclined Bodies of Revolution. NACA RM A50L07, 1951.

TABLE I.- GEOMETRIC CHARACTERISTICS OF MODEL

Fuselage:

Length, in. (cm)	50.56	(128.42)
Maximum cross-sectional area, sq ft (m^2)	0.0641	(0.0059)
Base area, sq ft (m^2)	0.0473	(0.0043)
Fineness ratio	14.7	

x		Diameter	
in.	cm	in.	cm
0	0	0	0
1	2.54	.52	1.32
2	5.08	1.00	2.54
3	7.62	1.52	3.86
4	10.16	1.96	4.98
5	12.70	2.34	5.95
6	15.24	2.66	6.76
7	17.78	2.93	7.44
8	20.23	3.16	8.03
9	22.86	3.33	8.46
10	25.40	3.42	8.69
11	27.94	3.43	8.71
26.54	67.41	3.43	8.71
26.54	67.41	3.41	8.66
45.33	115.14	3.41	8.66
50.56	128.42	2.95	7.49

Fins:

Fin 1 –

Tip chord, in. (cm)	1.82	(4.62)
Chord at body juncture, in.	6.00	(15.24)
Semispan, in. (cm)	4.19	(10.64)
Thickness ratio, t/c –		
Body juncture	0.046	
Tip	0.053	
Exposed planform area of one fin panel, sq in. (cm^2)	10.20	(65.79)
Airfoil section	Double wedge	

Fin 2 –

Chord at body juncture, in. (cm)	6.00	(15.24)
Semispan, in. (cm)	4.19	(10.64)
Thickness ratio, t/c –		
Body juncture	0.046	
Exposed planform area of one fin panel, sq in. (cm^2)	9.63	(62.11)
Airfoil section	Double wedge	

Fin 3 –

Tip chord, in. (cm)	3.60	(9.14)
Chord at body juncture, in. (cm)	6.00	(15.24)
Thickness ratio, t/c –		
Body juncture	0.045	
Tip	0.028	
Exposed planform area of one fin panel, sq in. (cm^2)	12.38	(79.85)
Airfoil section	Double wedge	

Fin 4 –

Chord at body juncture, in. (cm)	6.00	(15.24)
Semispan, in. (cm)	4.19	(10.64)
Thickness ratio, t/c –		
Body juncture	0.045	
Exposed planform area of one fin planform, sq in. (cm^2)	10.34	(66.69)
Airfoil section	Double wedge	

Fin 5 –

Chord at body juncture, in. (cm)	6.00	(15.24)
Semispan, in. (cm)	4.19	(10.64)
Thickness ratio, t/c –		
Body juncture	0.045	
Exposed planform area of one fin planform, sq in. (cm^2)	11.87	(76.56)
Airfoil section	Double wedge	

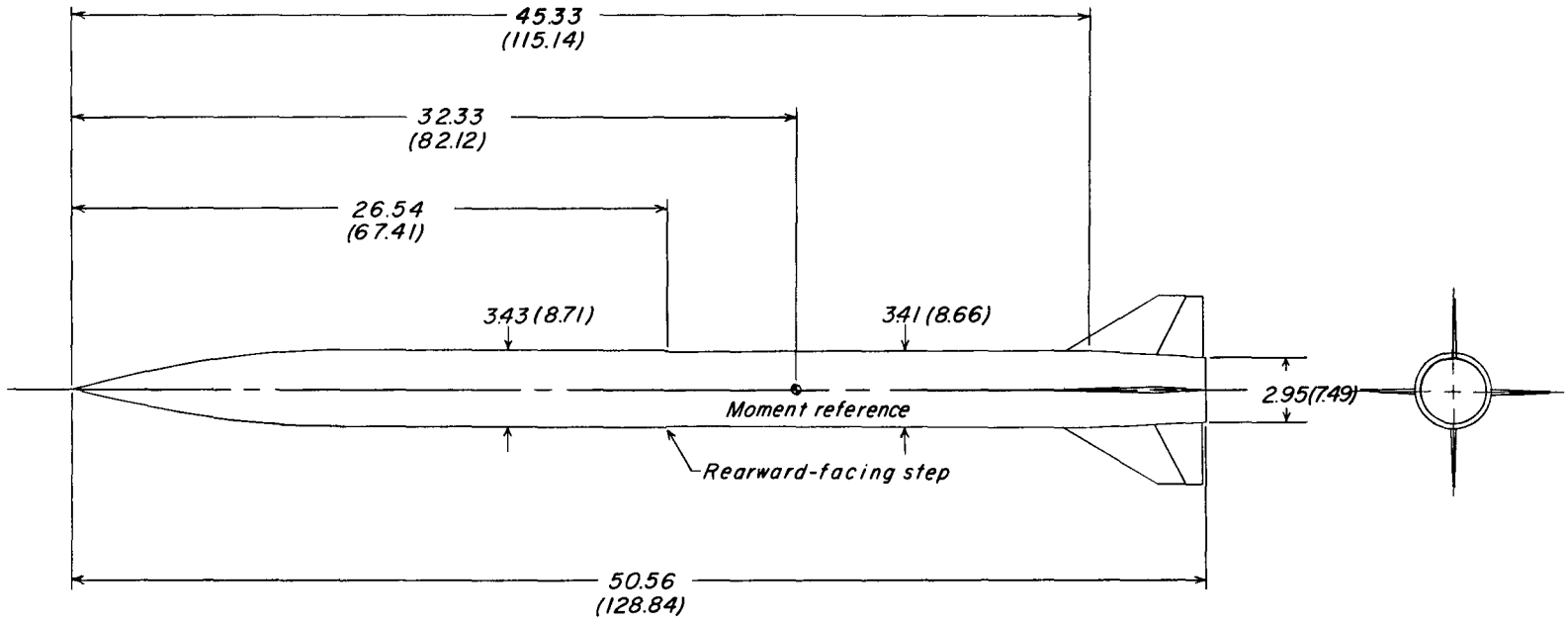

(a) Two-view drawing of configuration with fin 1 arrangement.

Figure 1.- Details of configuration. Dimensions are given first in inches and parenthetically in centimeters.

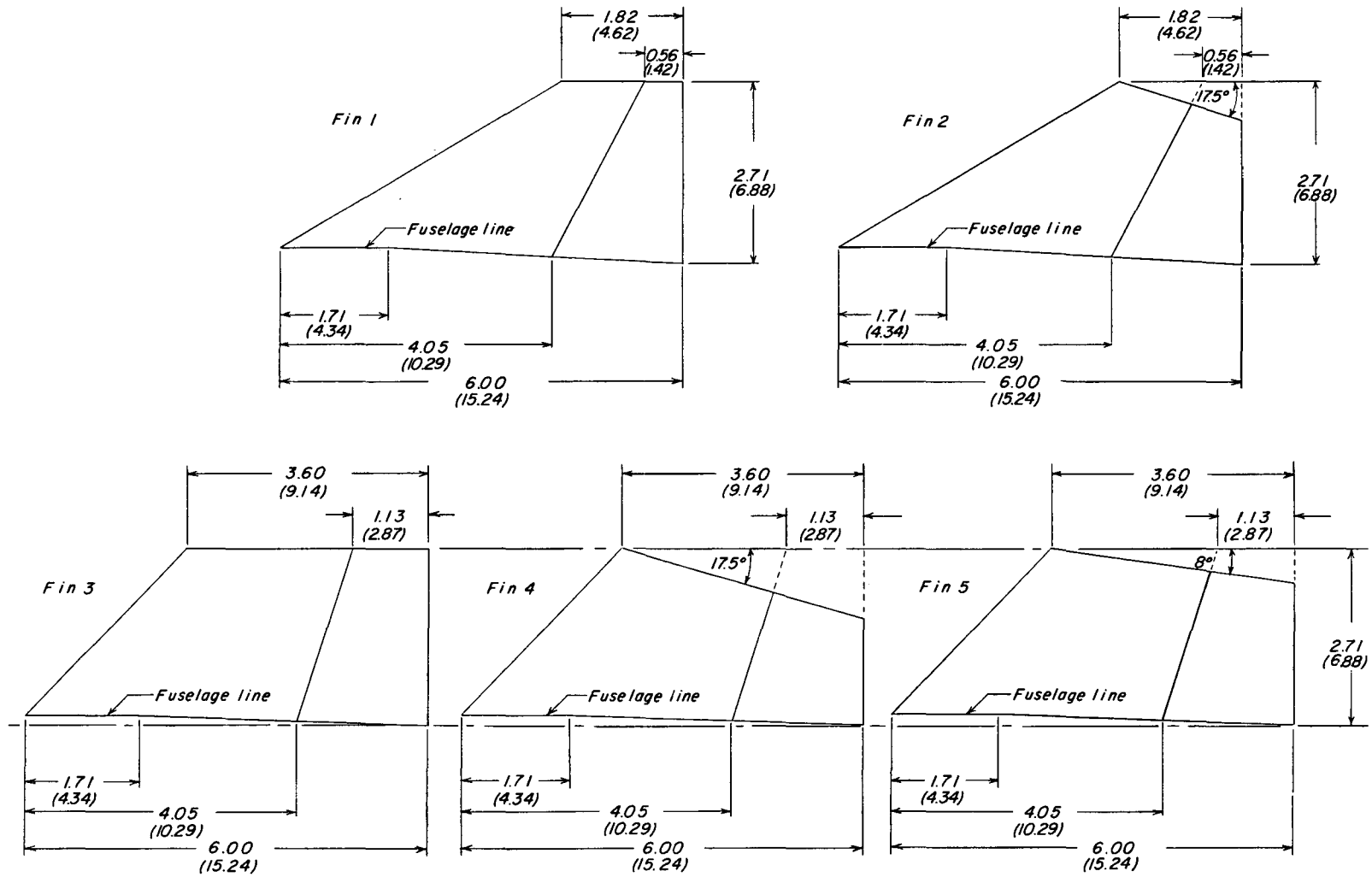

(b) Fin details.

Figure 1.- Concluded.

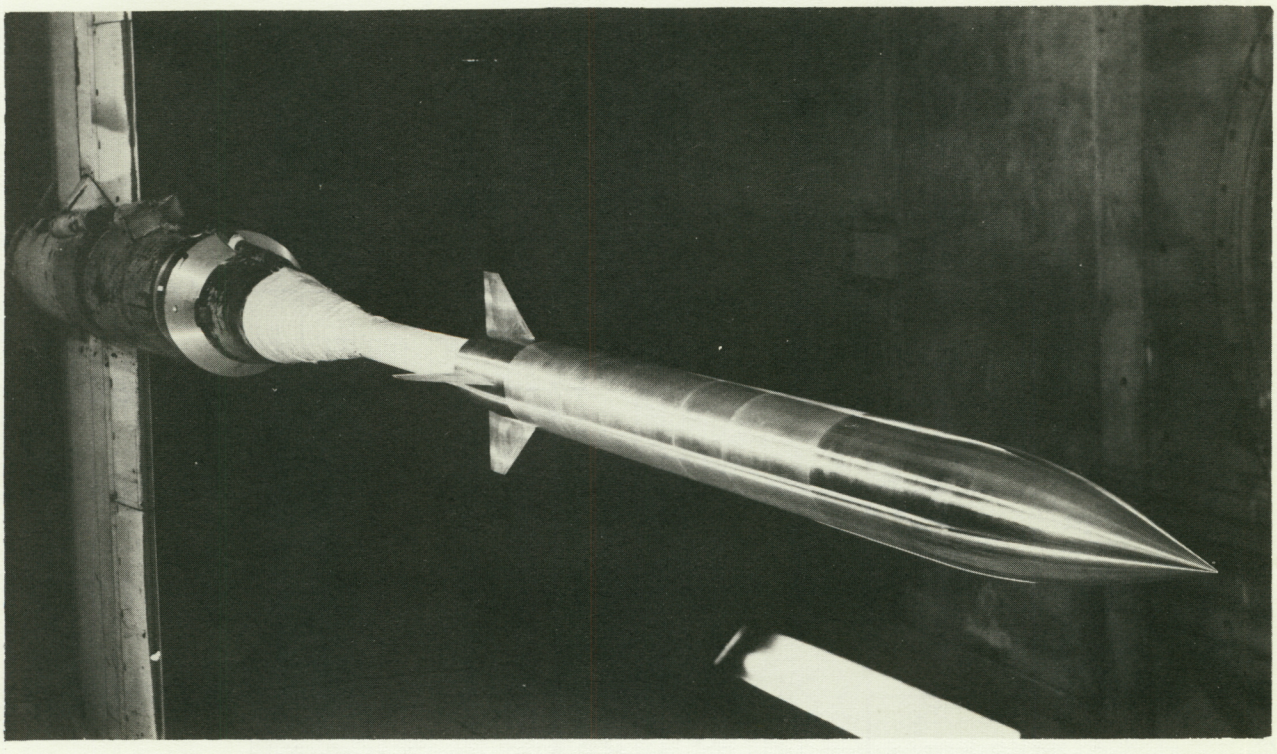

L-64-4623

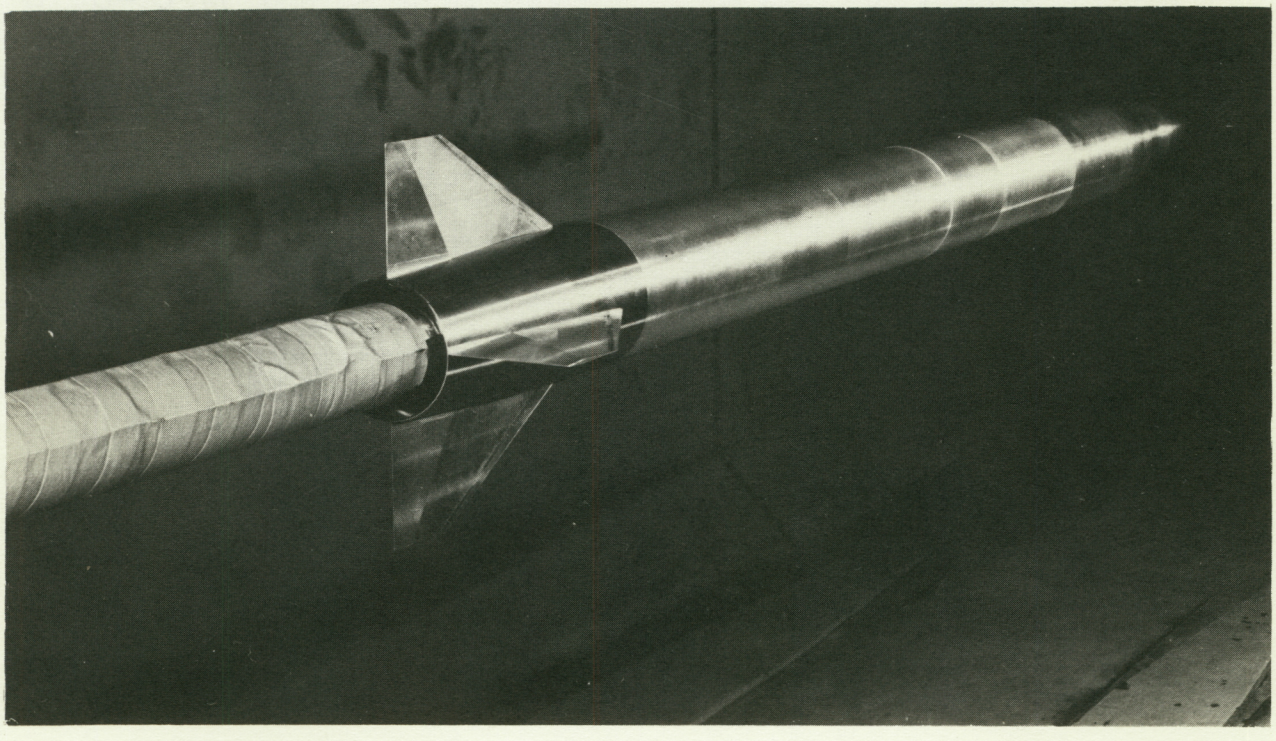

Figure 2.- Photographs of configuration with fin 1 arrangement. L-64-4621

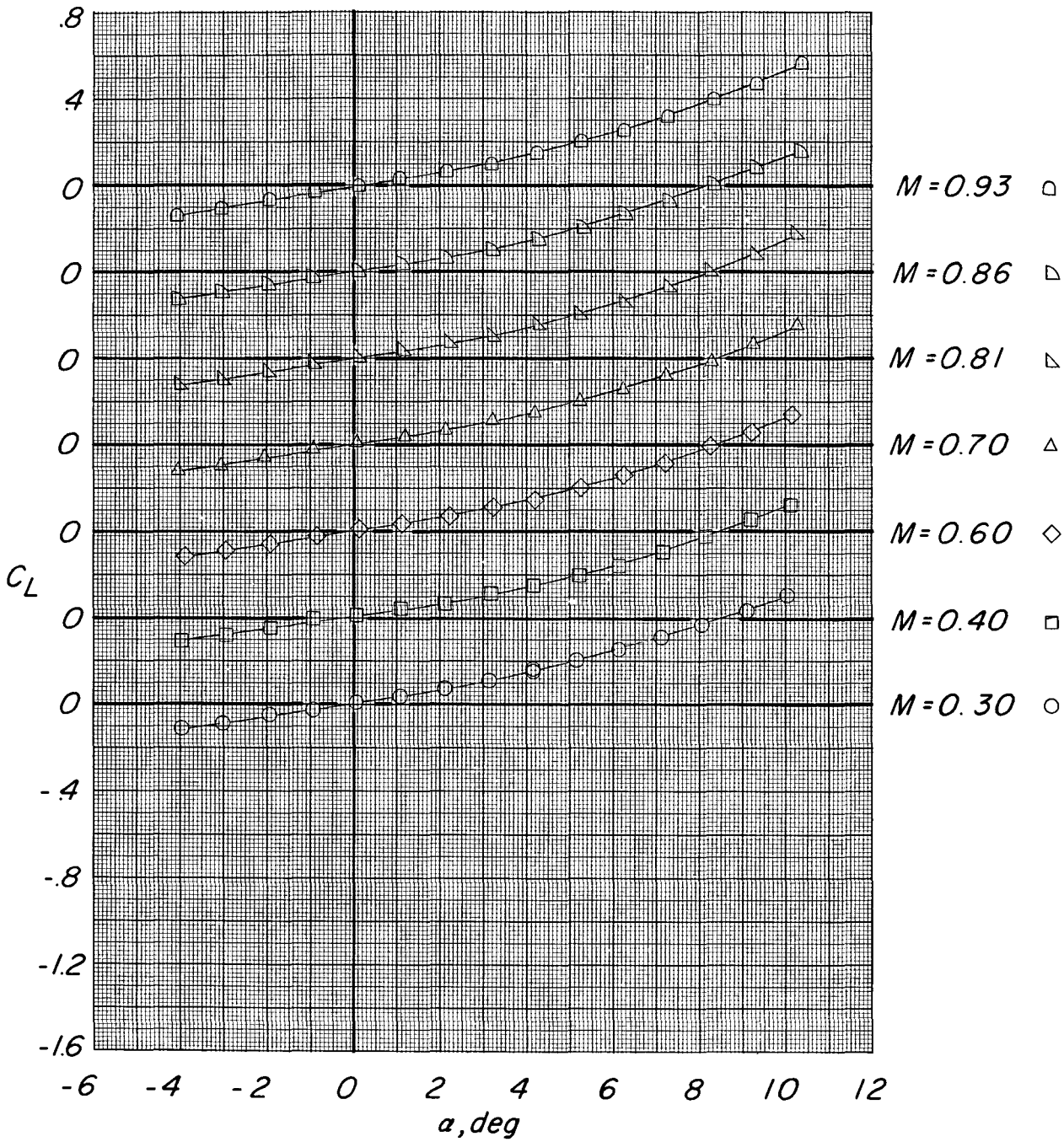

(a) Body alone.

Figure 3.- Variation of lift coefficient C_L with angle of attack α for test configurations. $\phi = 0^o$.

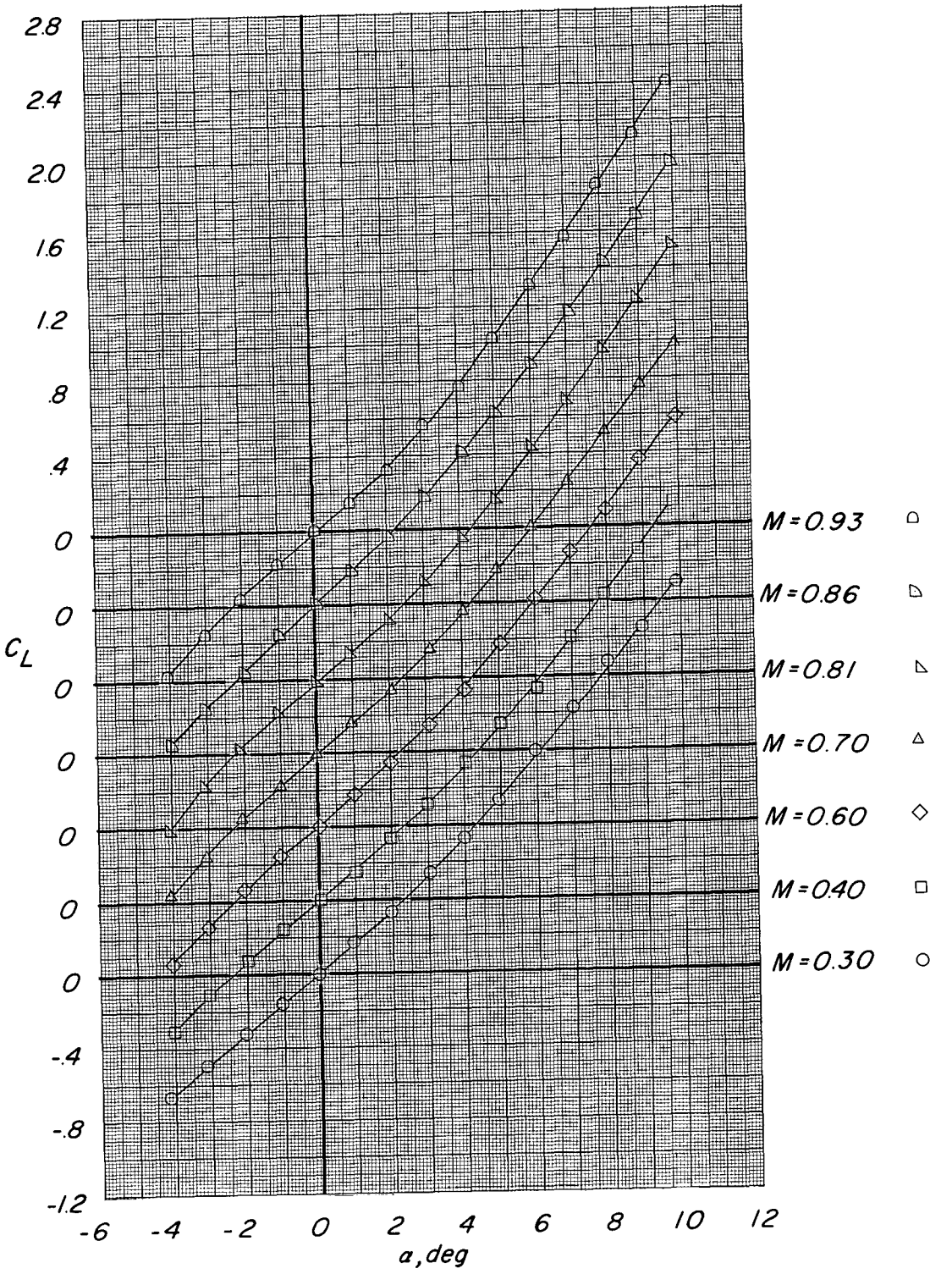

(b) Body with fin 1 arrangement.

Figure 3.- Continued.

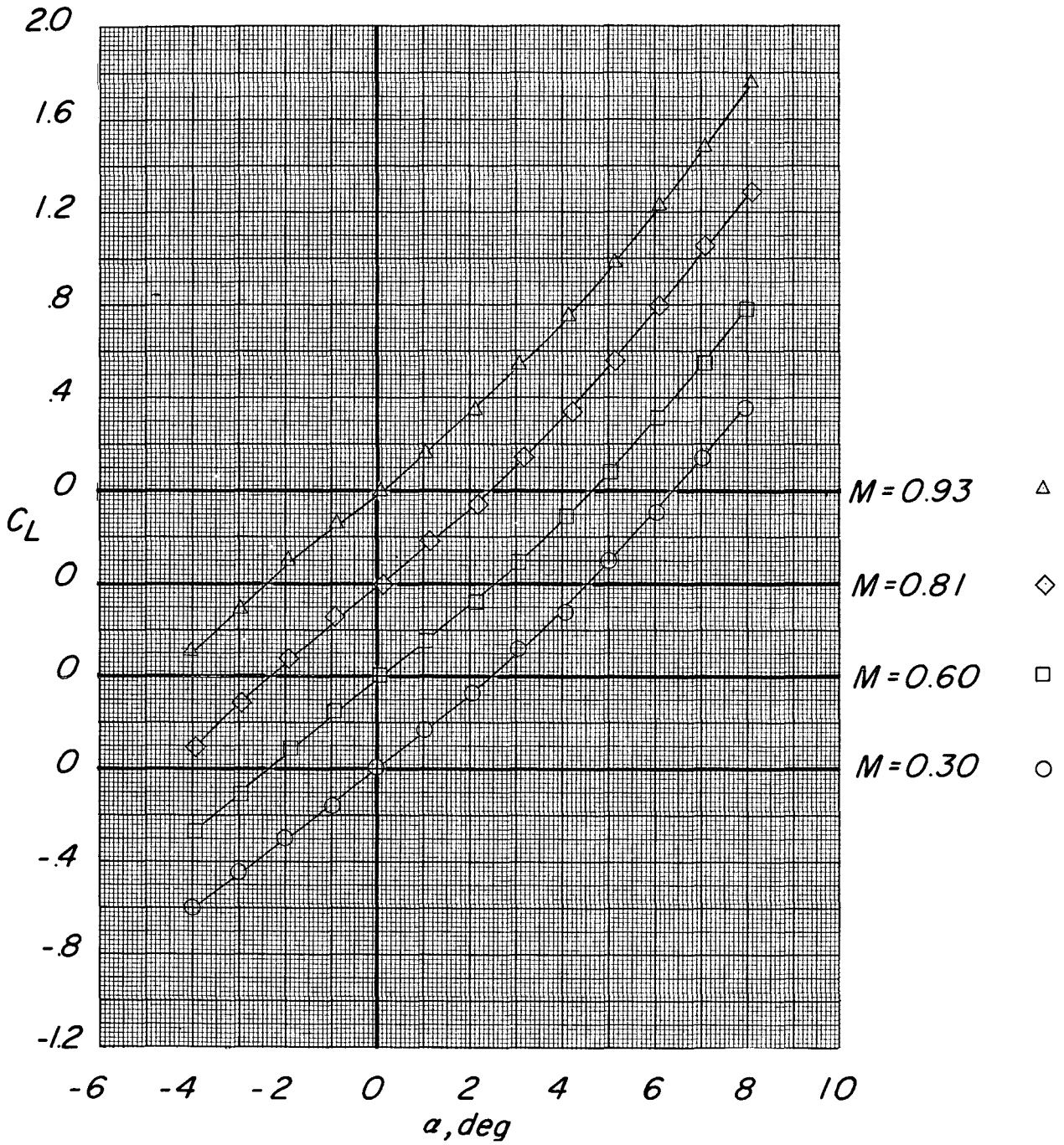

(c) Body with fin 2 arrangement.

Figure 3.- Continued.

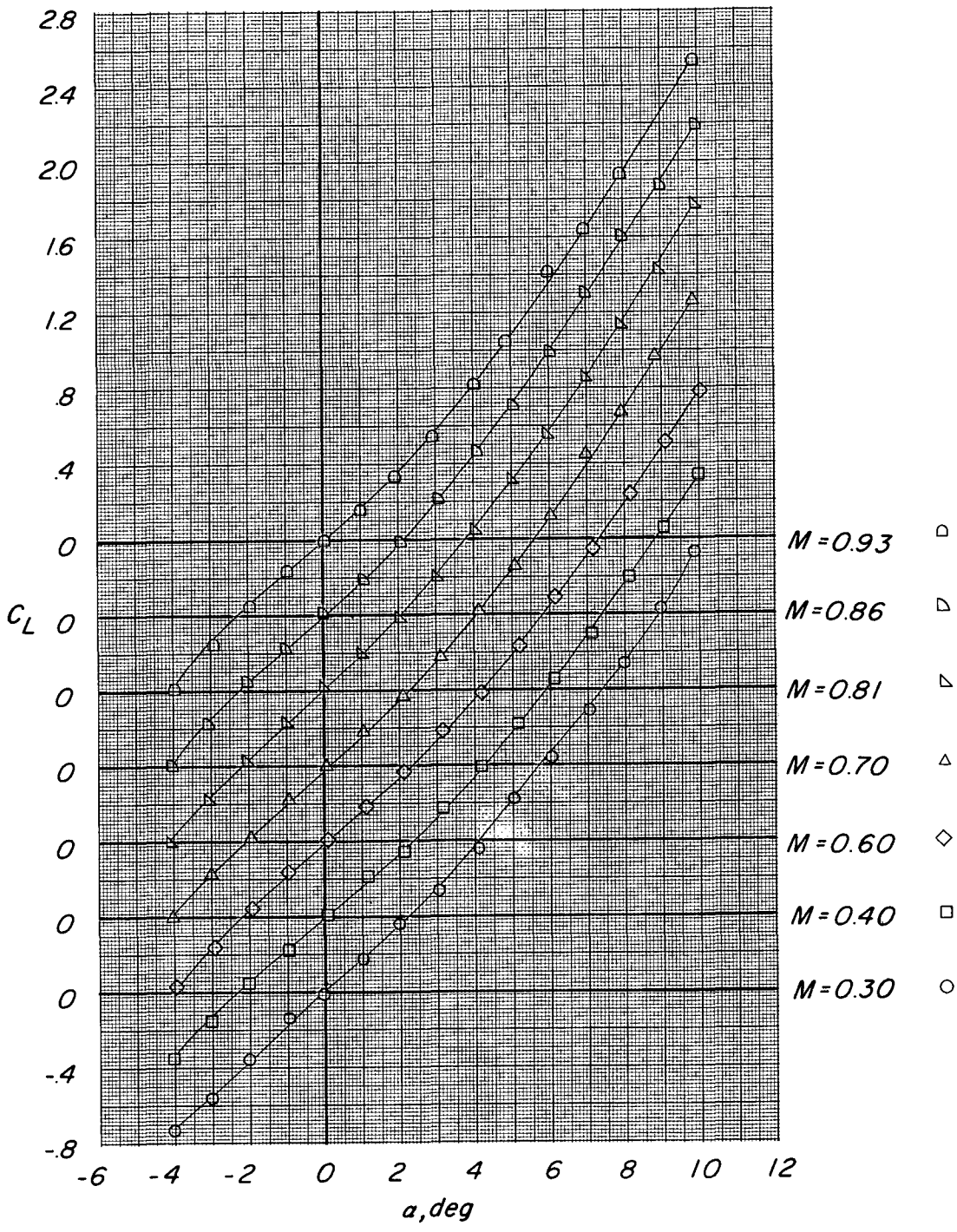

(d) Body with fin 3 arrangement.

Figure 3.- Continued.

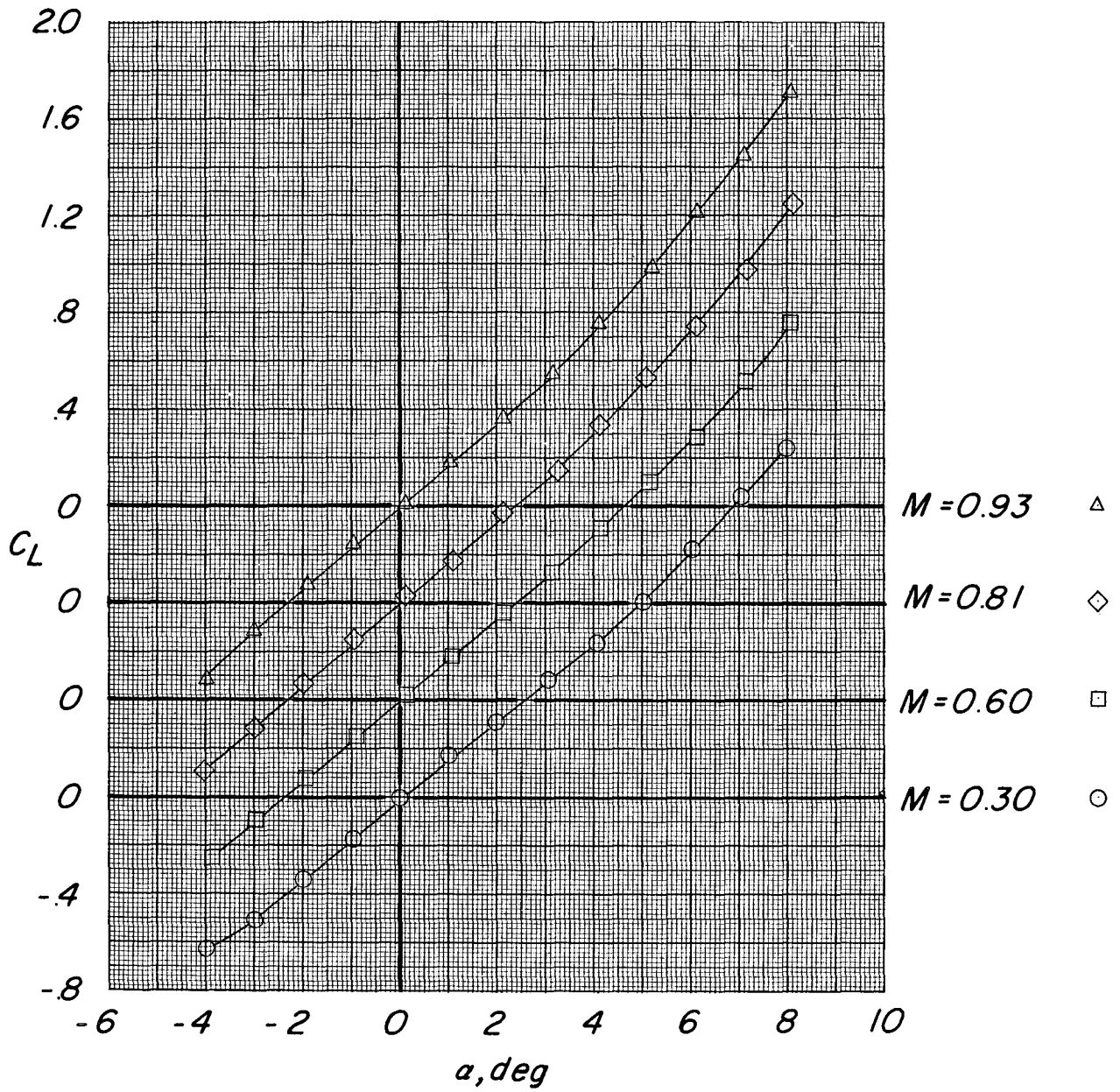

(e) Body with fin 4 arrangement.

Figure 3.- Continued.

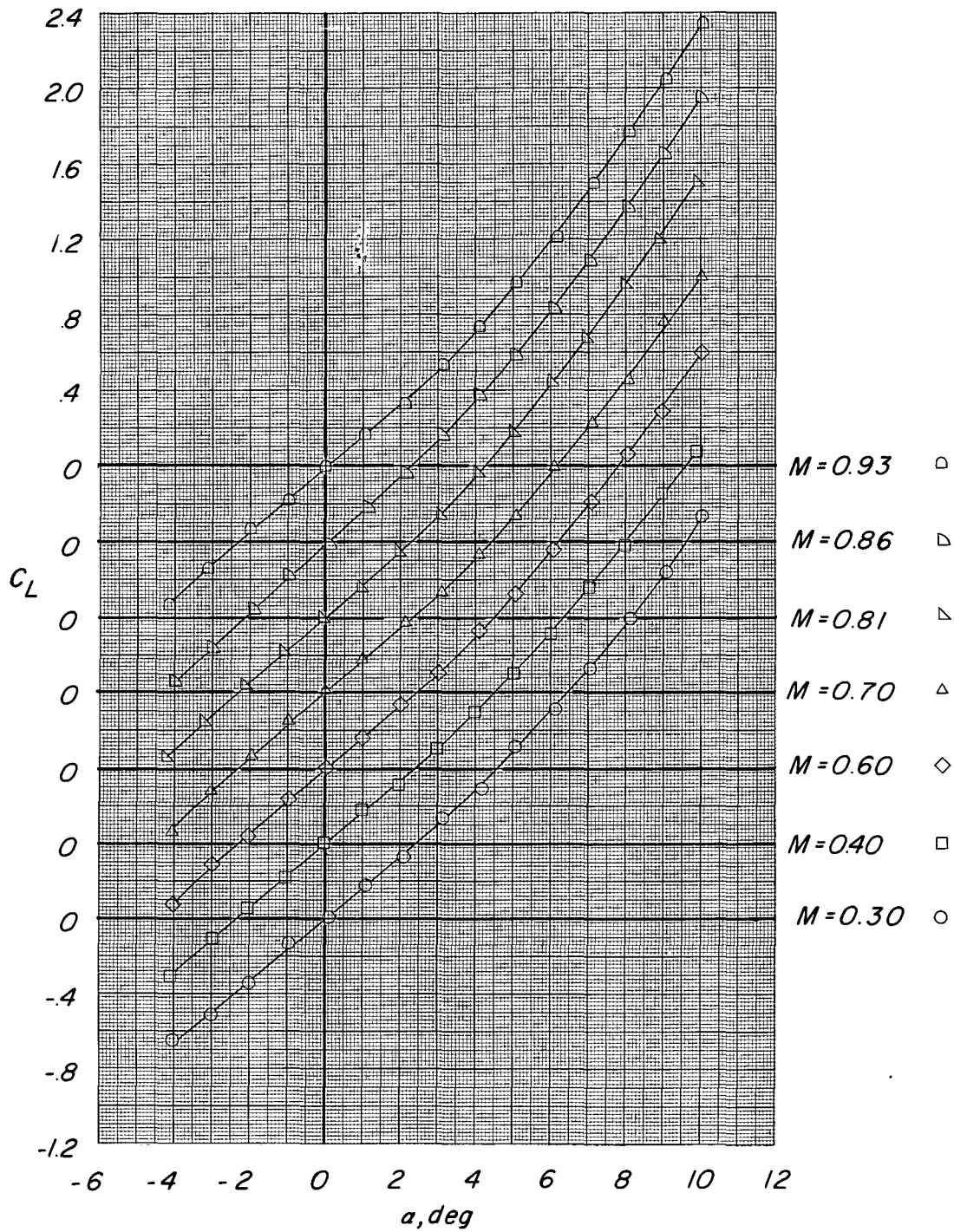

(f) Body with fin 5 arrangement.

Figure 3.- Concluded.

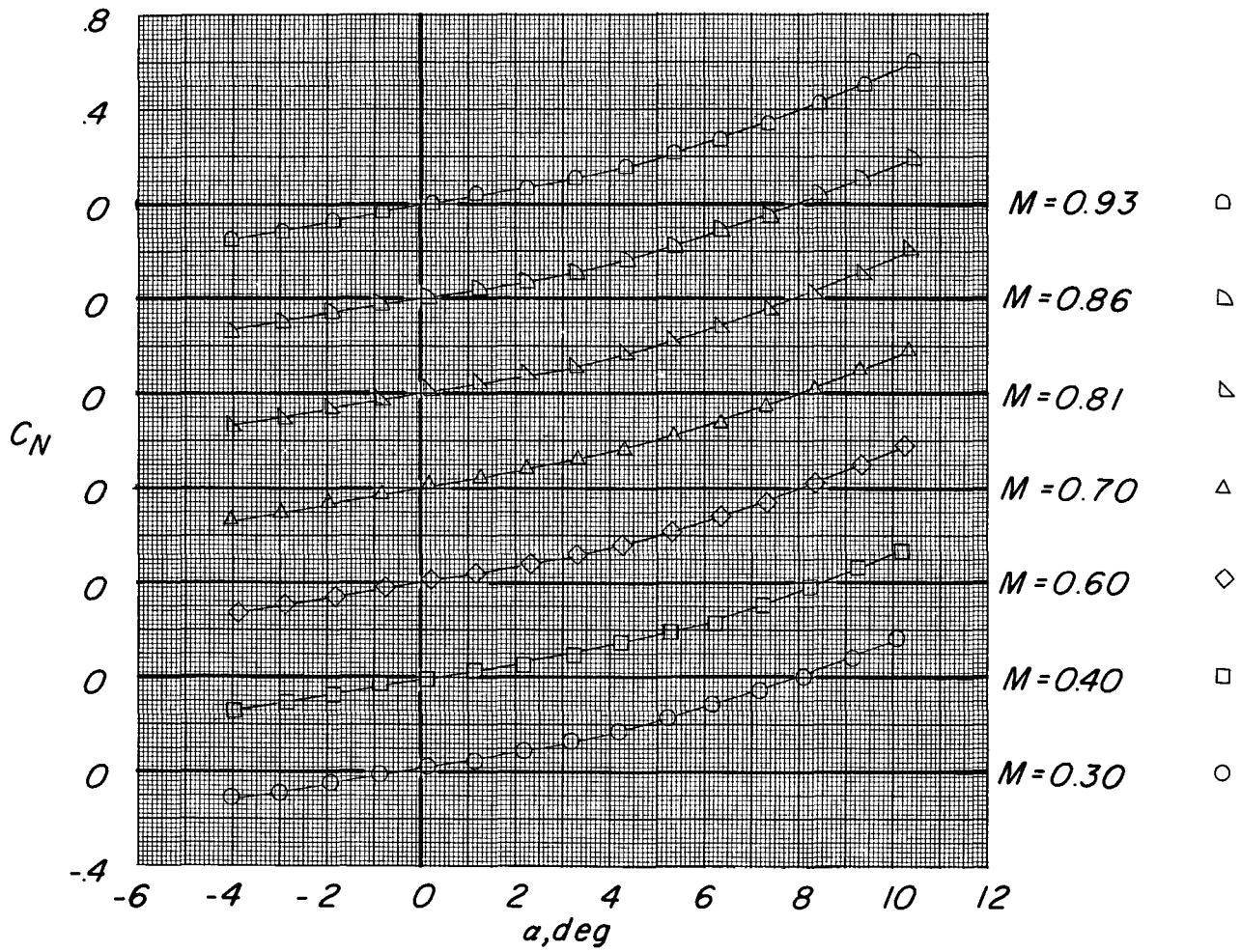

(a) Body alone.

Figure 4.- Variation of normal-force coefficient C_N with angle of attack α for test configurations. $\phi = 0^0$.

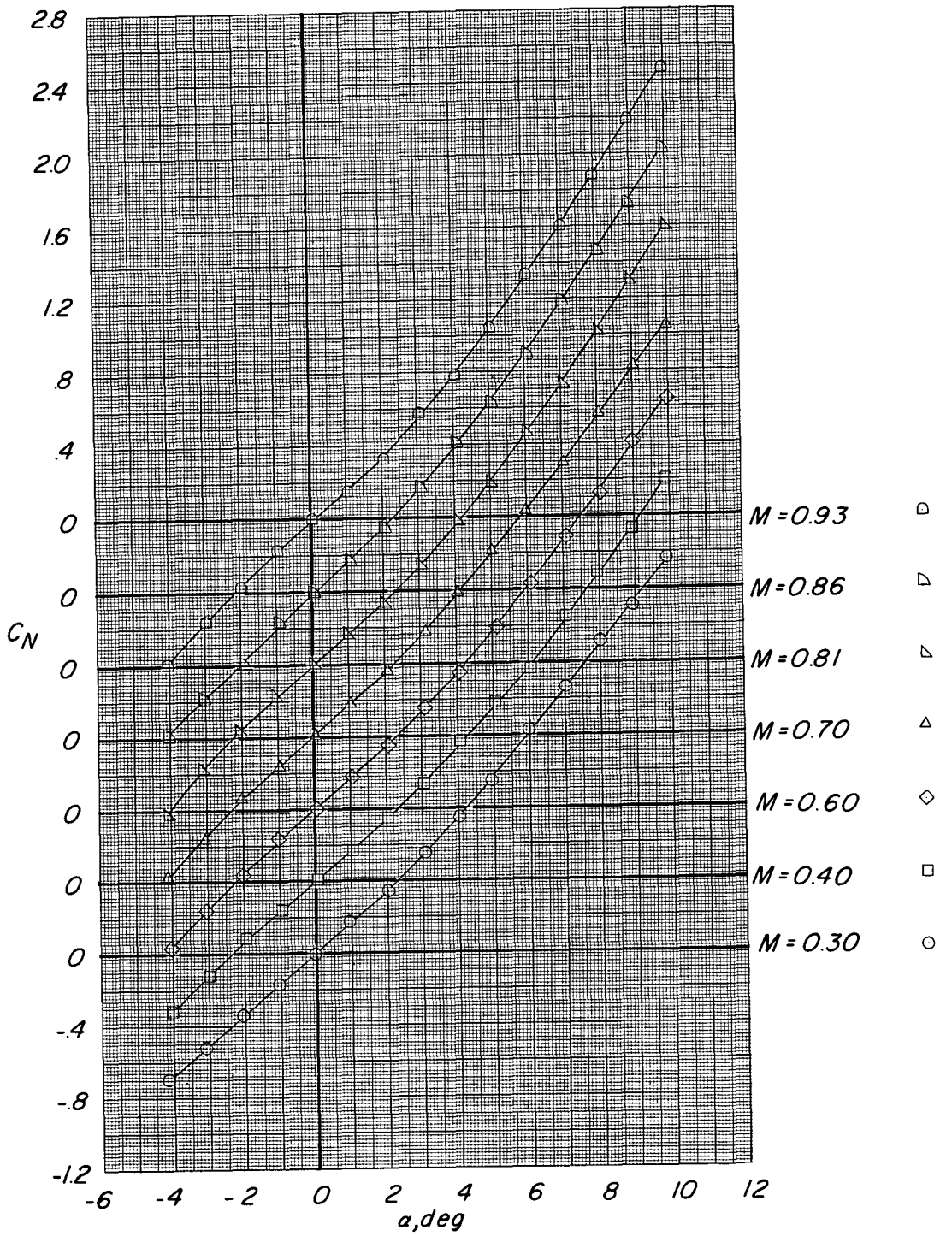

(b) Body with fin 1 arrangement.

Figure 4.- Continued.

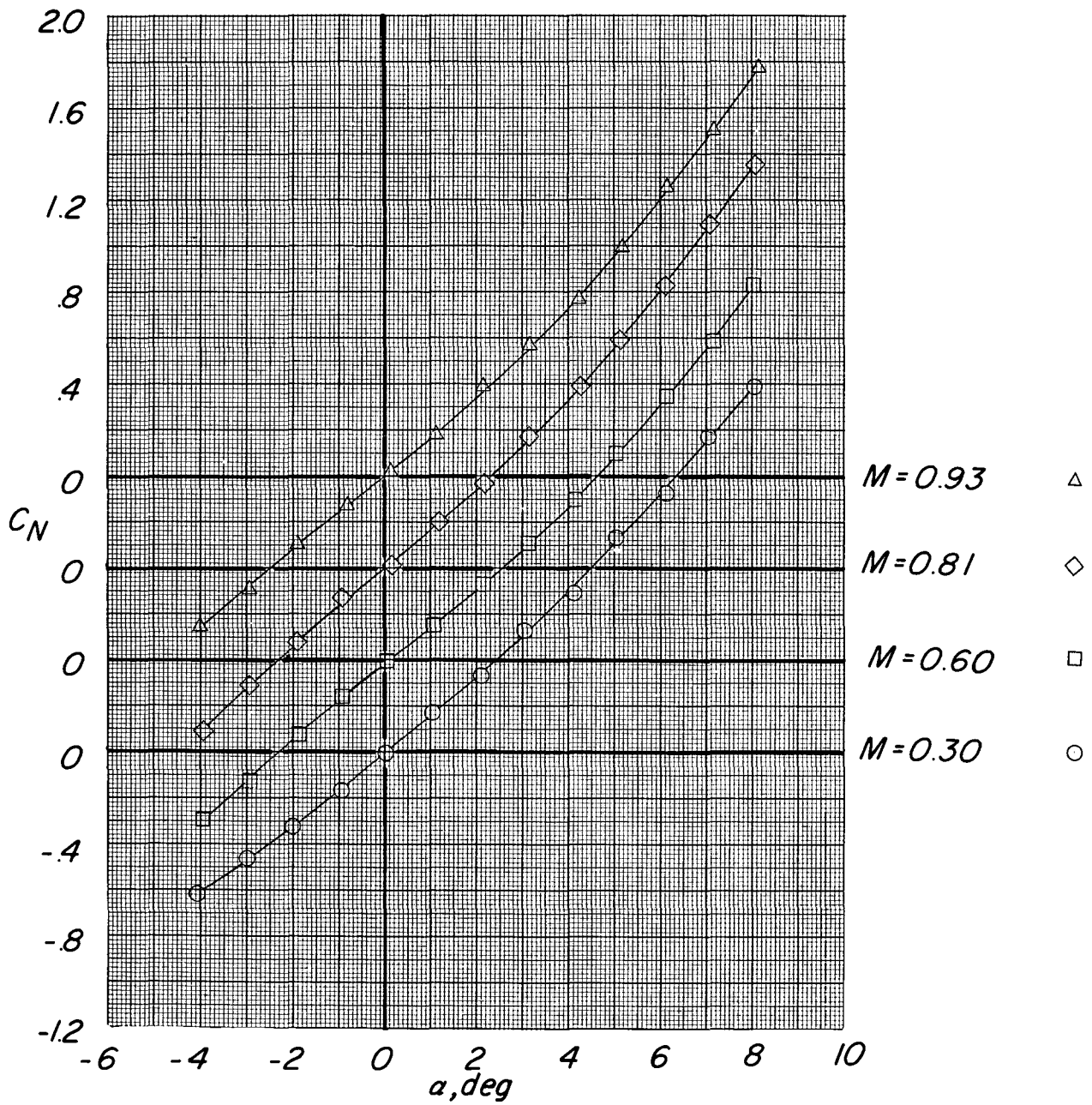

(c) Body with fin 2 arrangement.

Figure 4.- Continued.

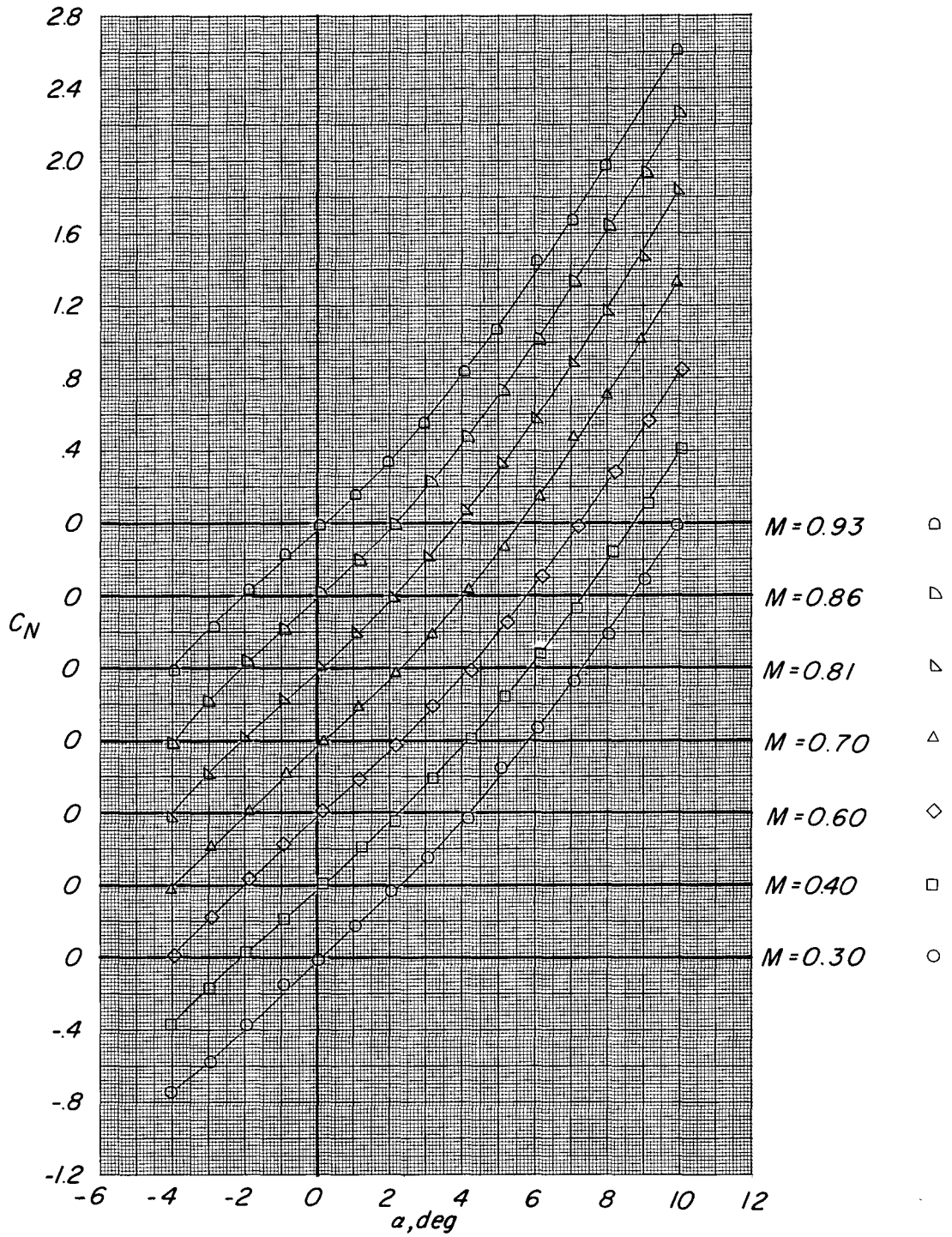

(d) Body with fin 3 arrangement.

Figure 4.- Continued.

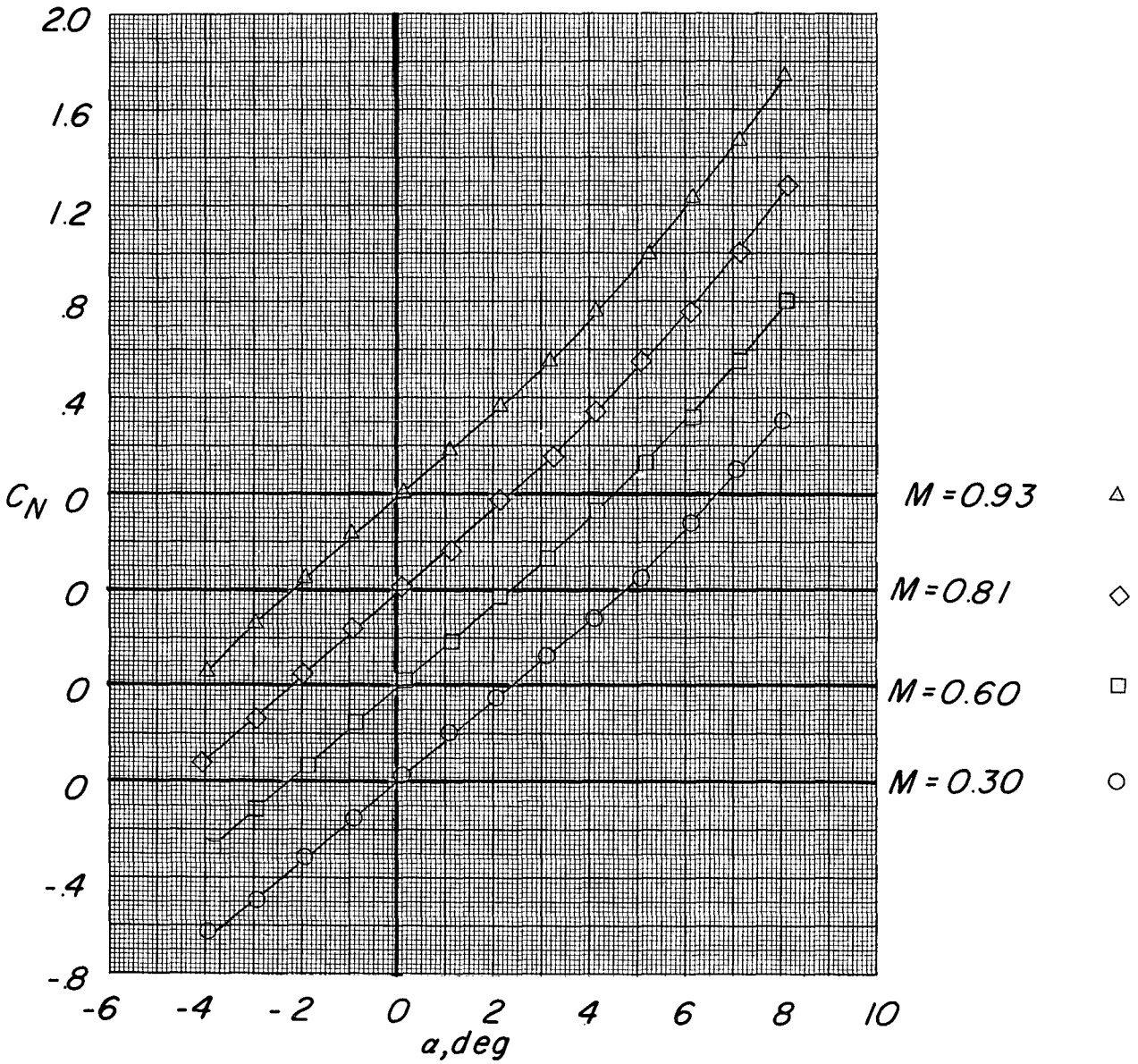

(e) Body with fin 4 arrangement.

Figure 4.- Continued.

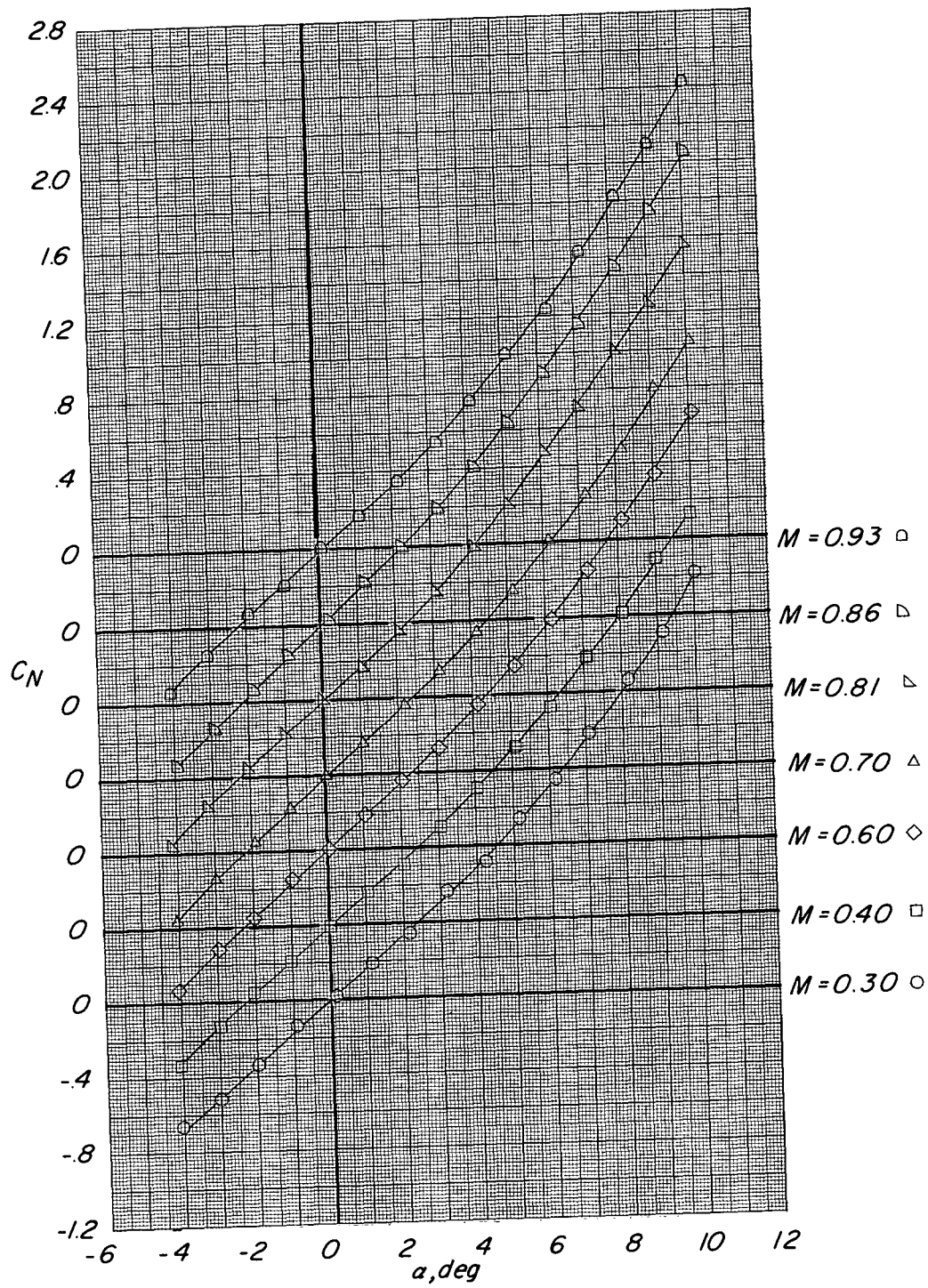

(f) Body with fin 5 arrangement.

Figure 4.- Concluded.

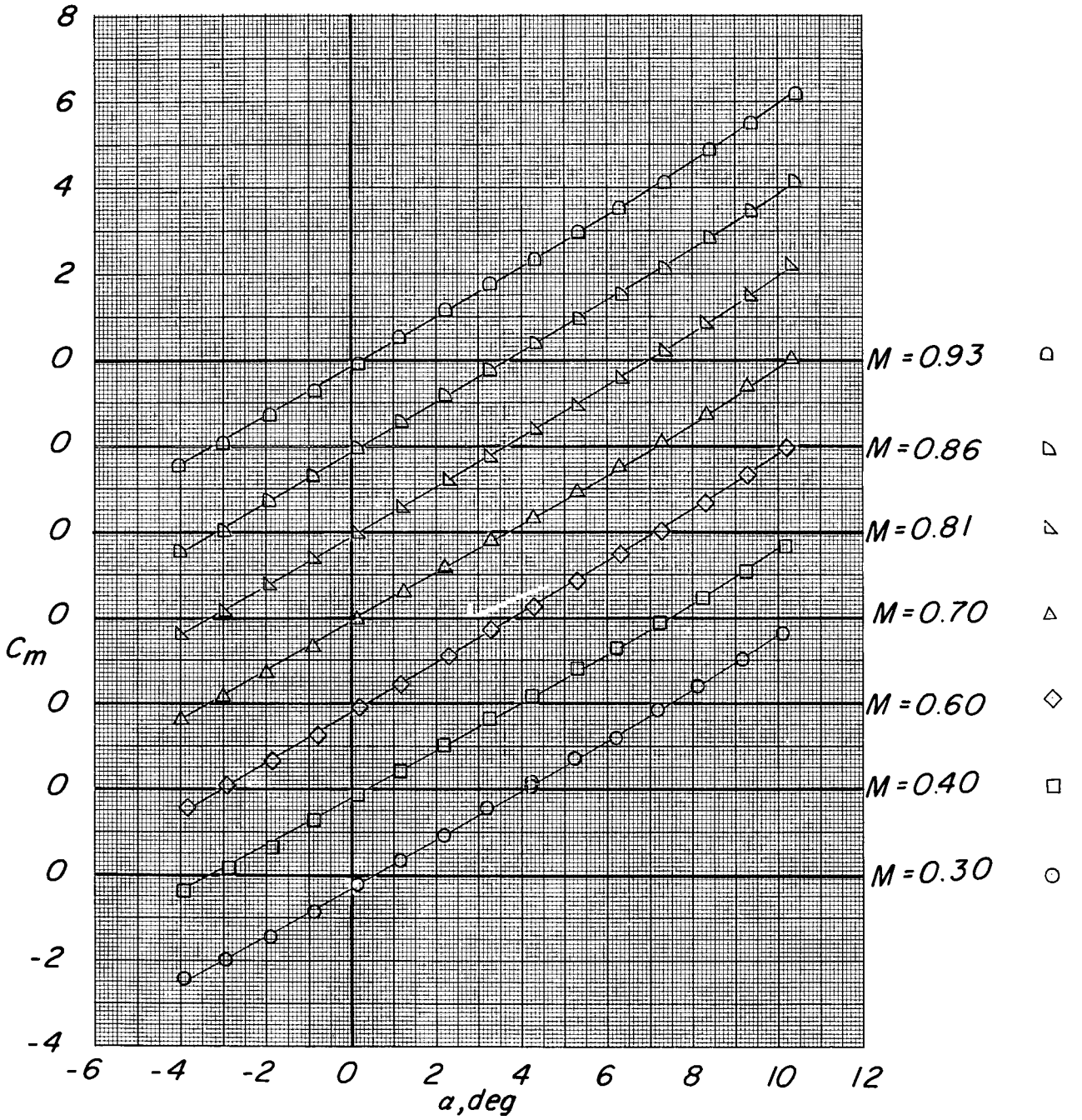

(a) Body alone.

Figure 5.- Variation of pitching-moment coefficient C_m with angle of attack α for test configurations. $\phi = 0^o$.

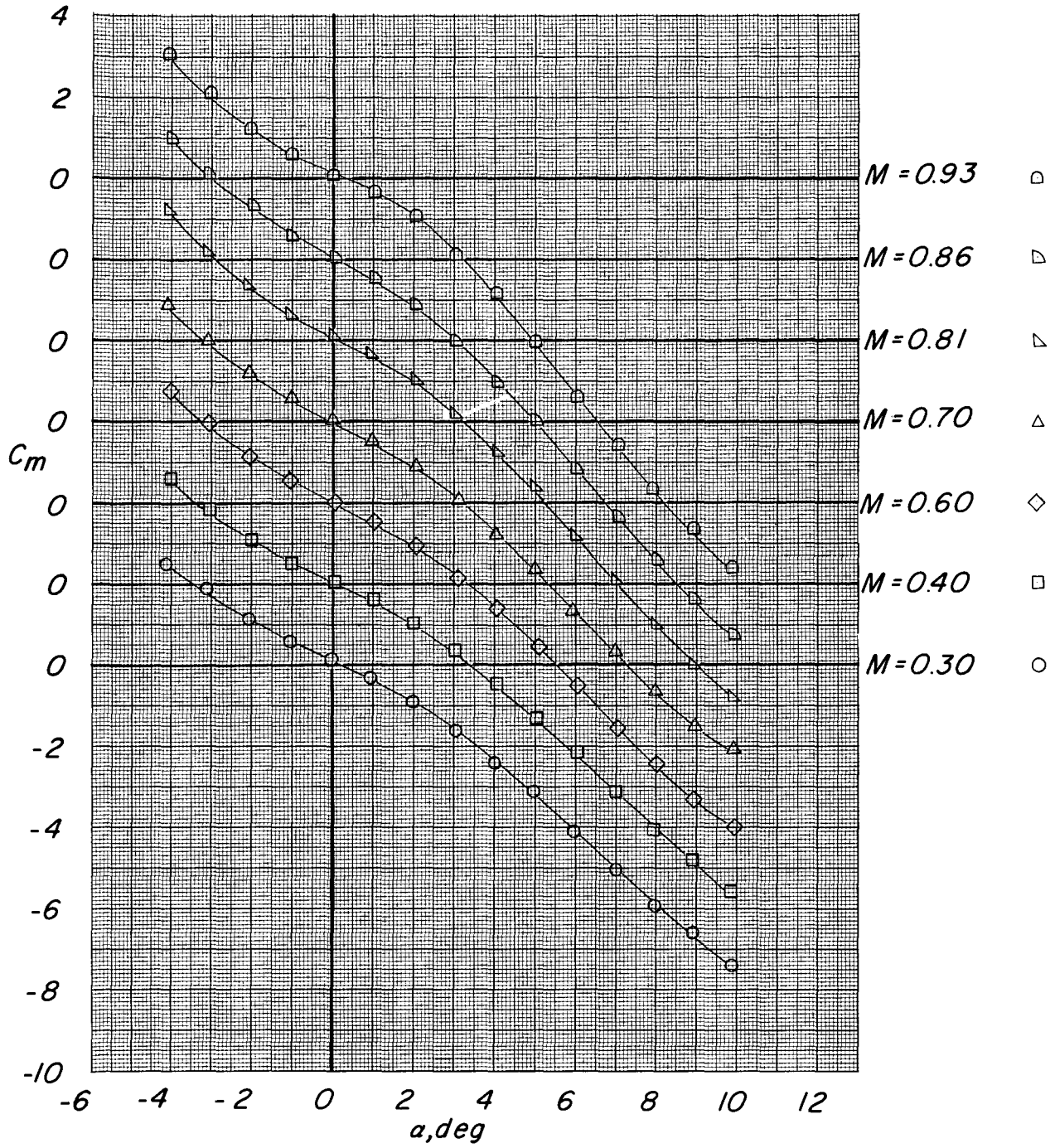

(b) Body with fin 1 arrangement.

Figure 5.- Continued.

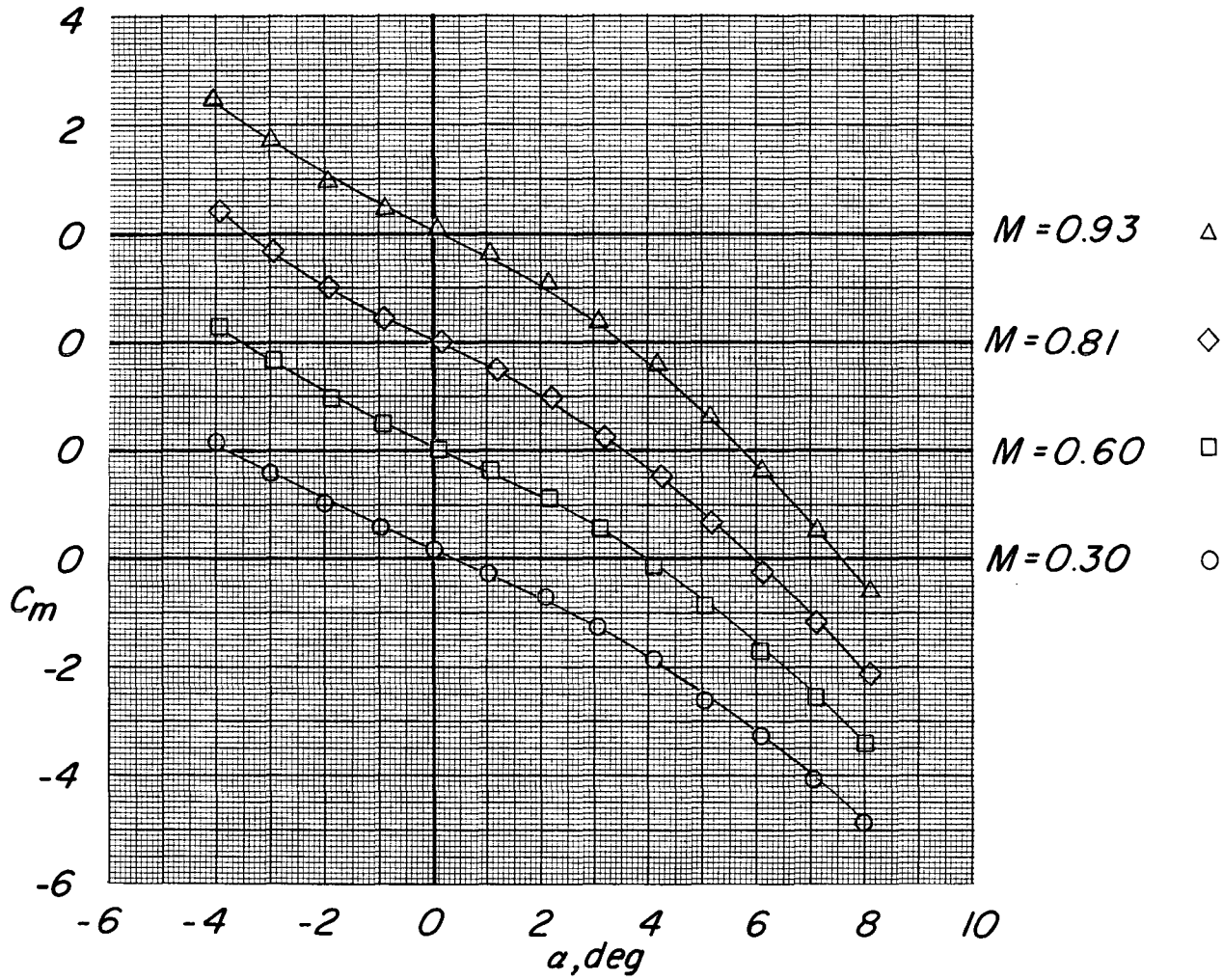

(c) Body with fin 2 arrangement.

Figure 5.- Continued.

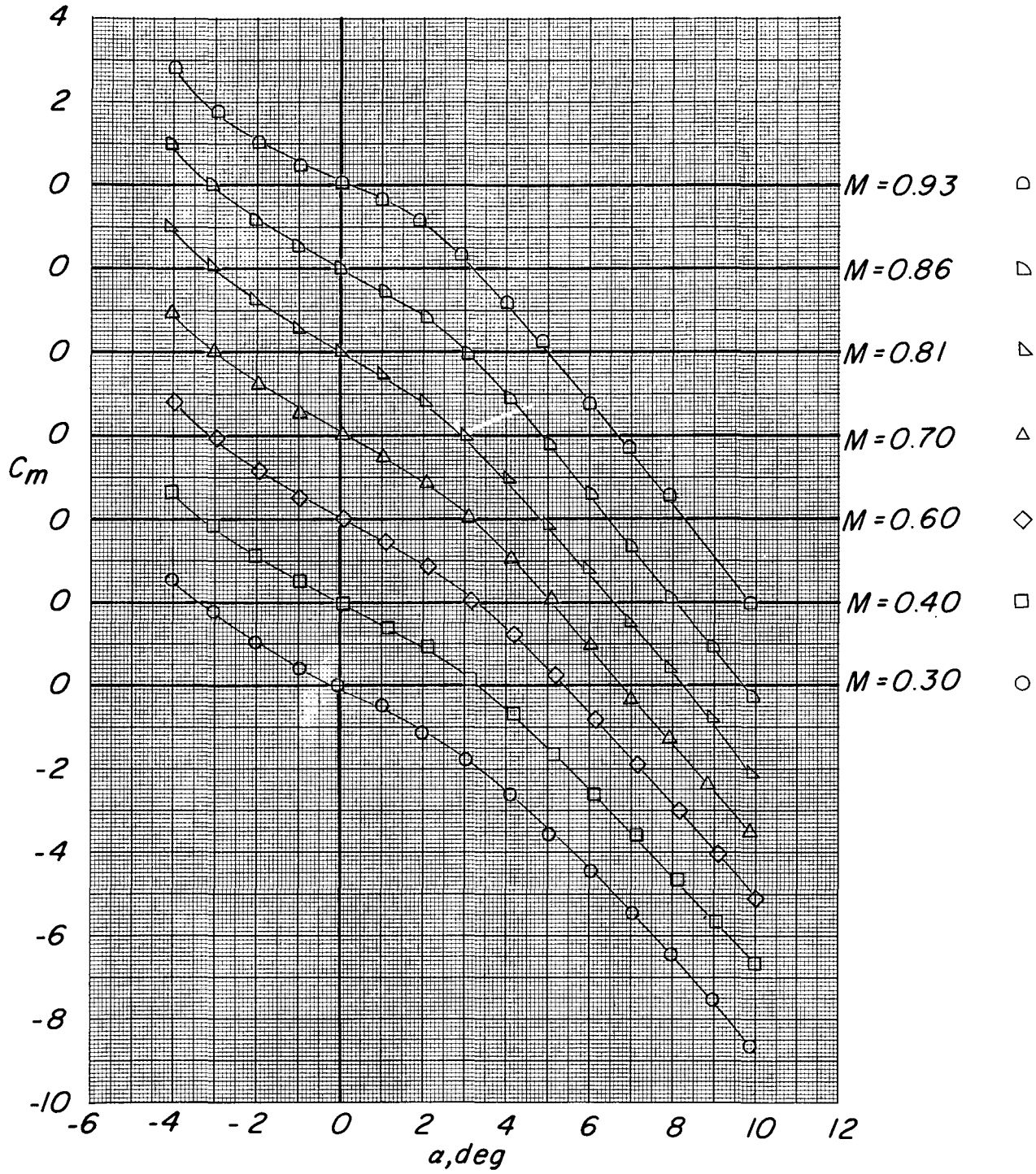

(d) Body with fin 3 arrangement.

Figure 5.- Continued.

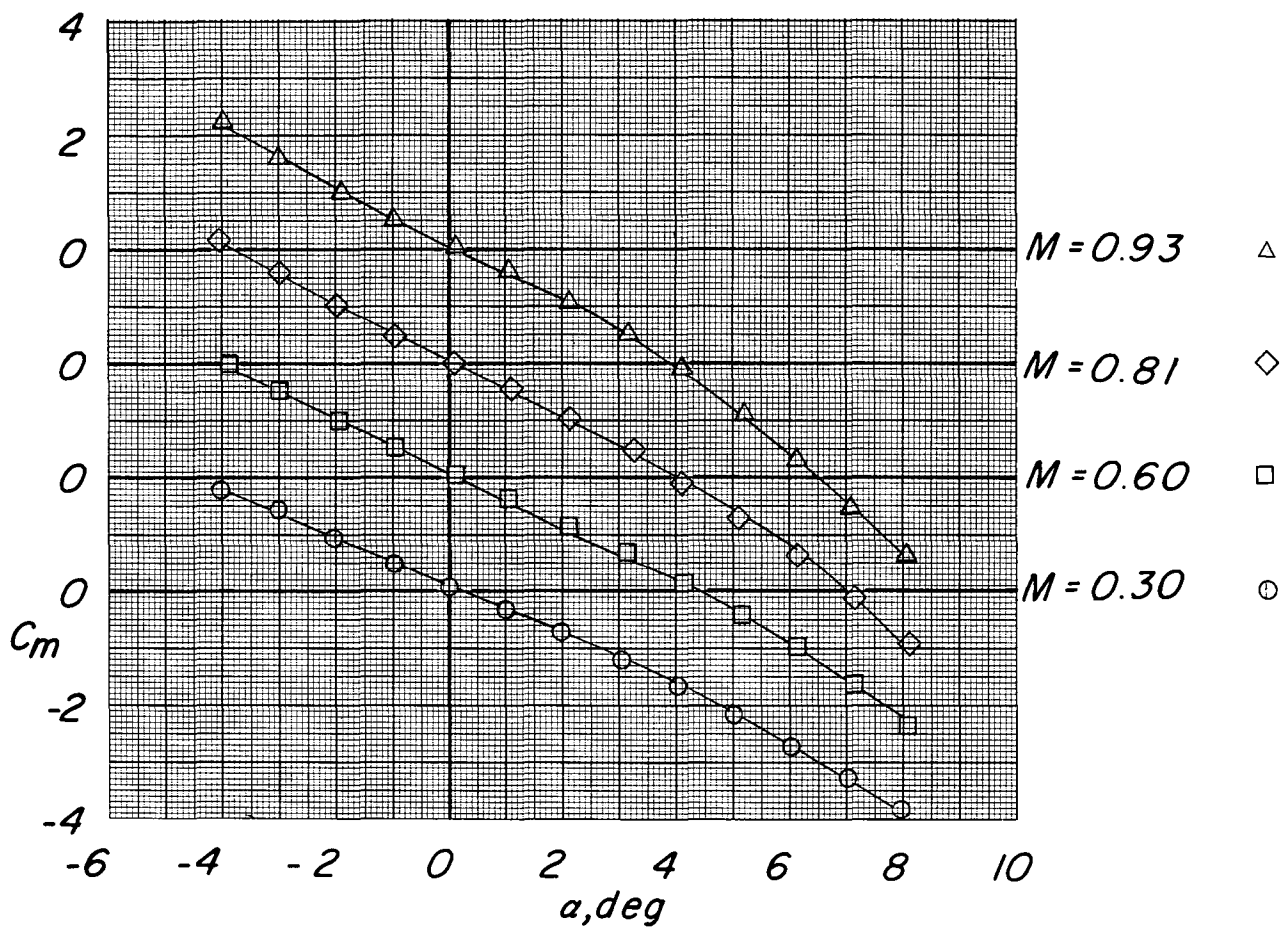

(e) Body with fin 4 arrangement.

Figure 5.- Continued.

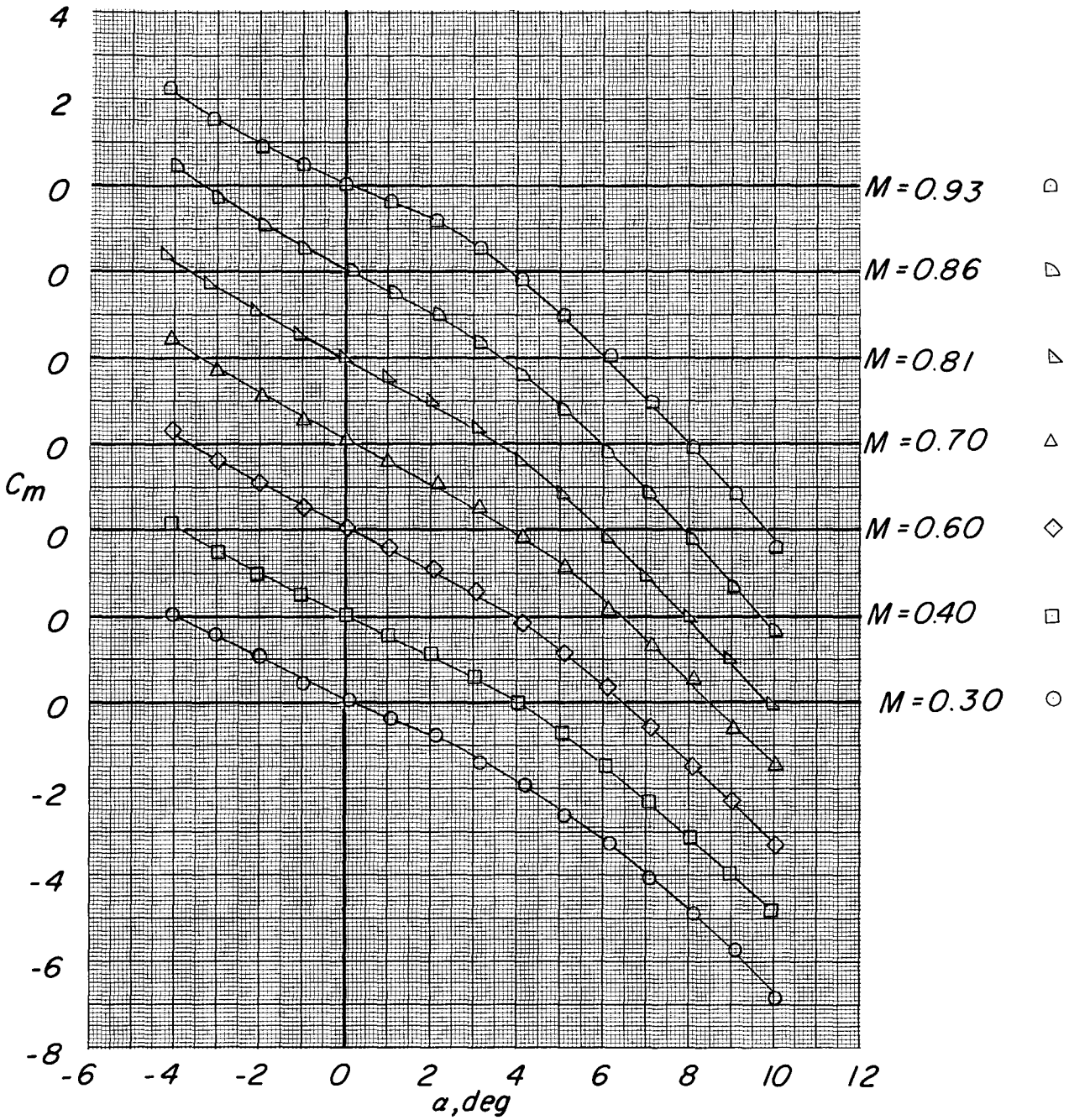

(f) Body with fin 5 arrangement.

Figure 5.- Concluded.

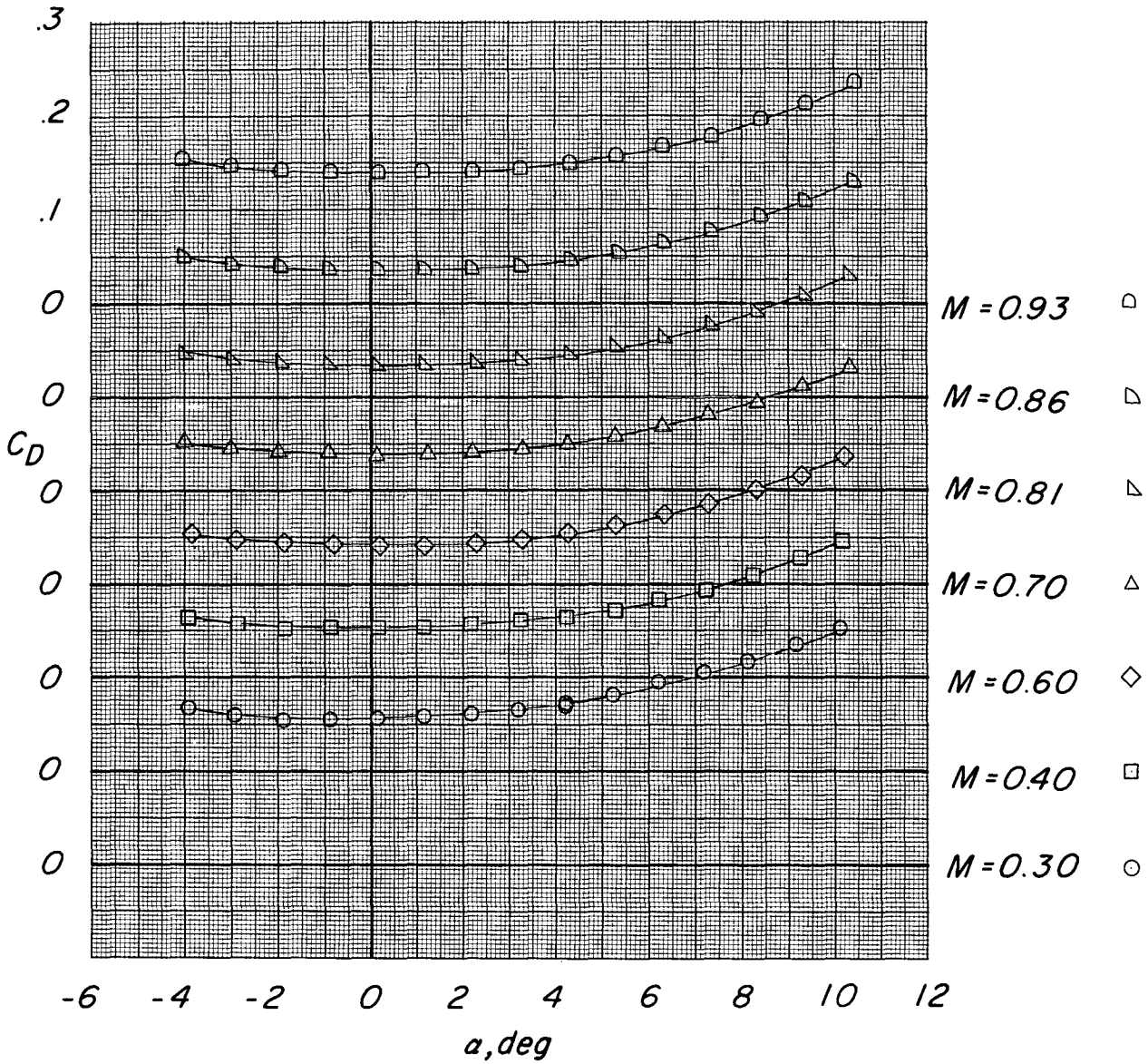

(a) Body alone.

Figure 6.- Variation of drag coefficient C_D with angle of attack α for test configurations. $\phi = 0^o$.

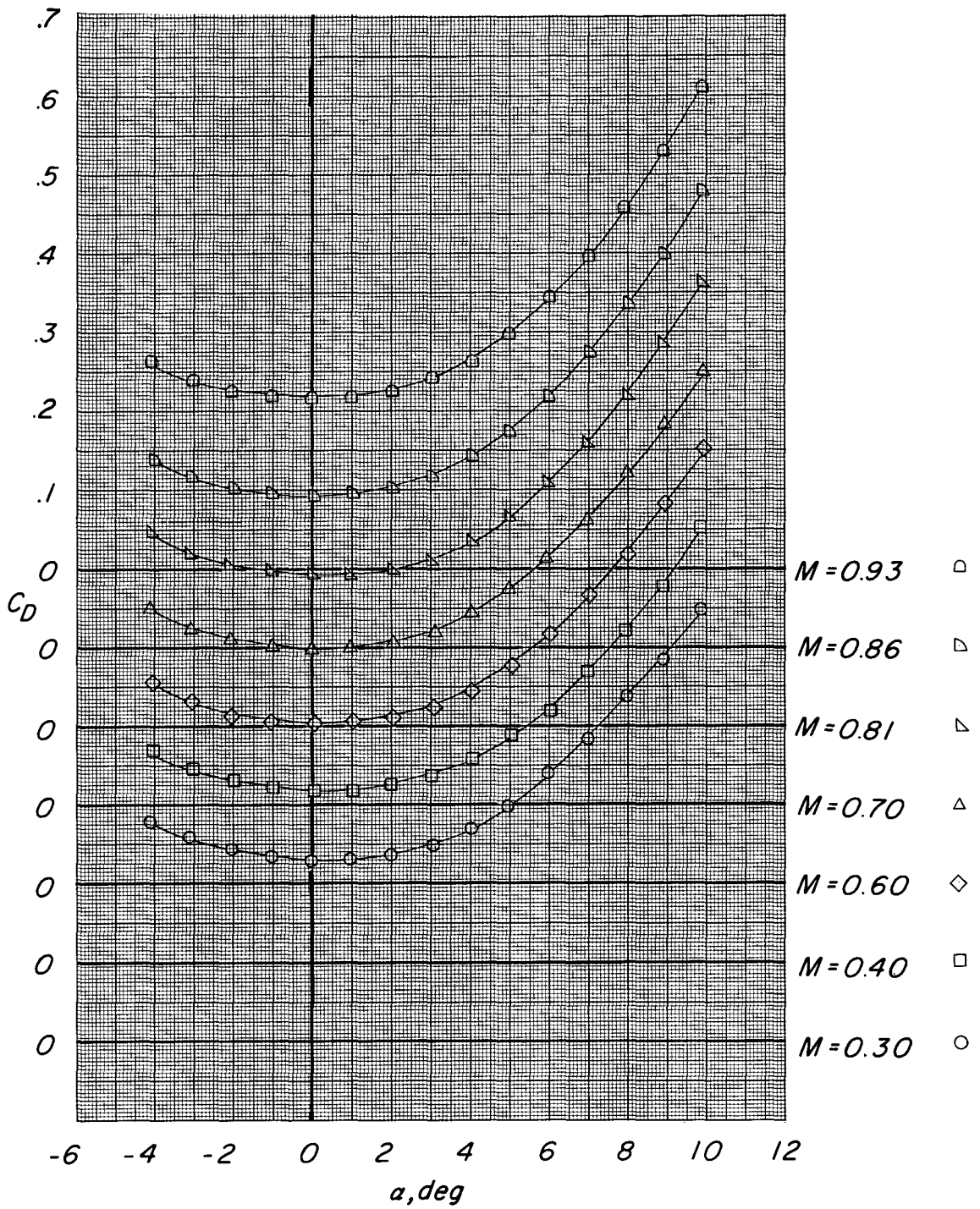

(b) Body with fin 1 arrangement.

Figure 6.- Continued.

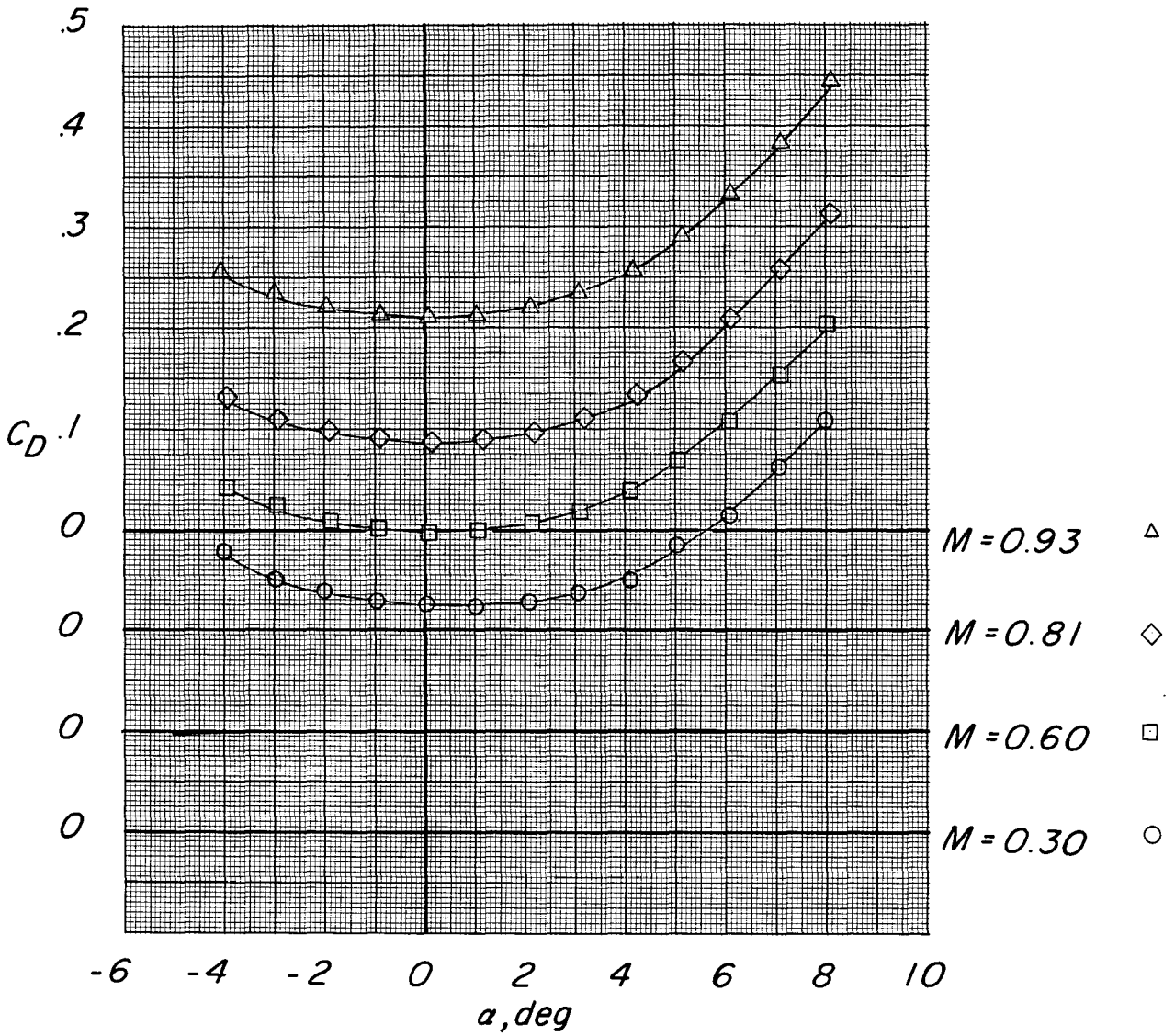

(c) Body with fin 2 arrangement.

Figure 6.- Continued.

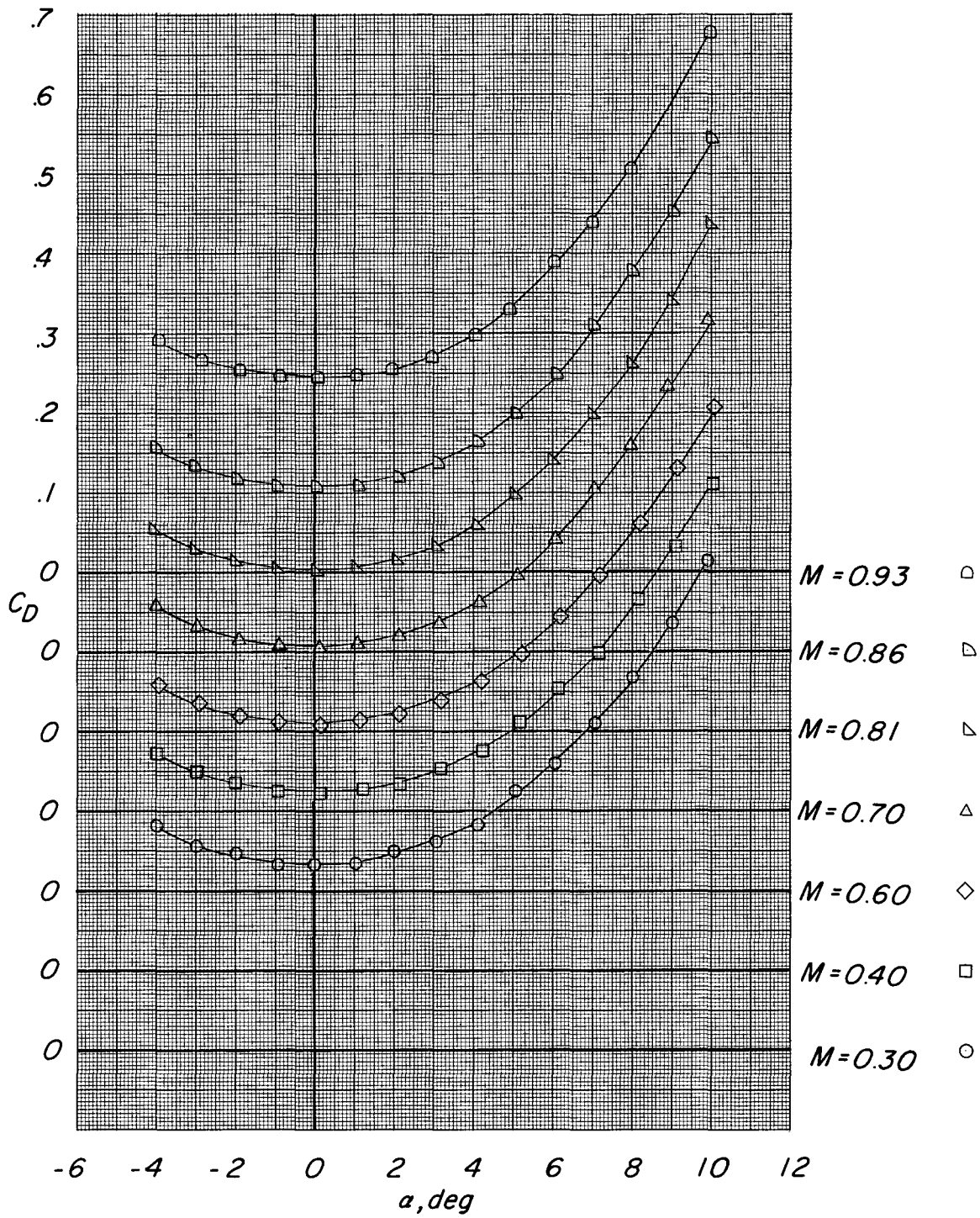

(d) Body with fin 3 arrangement.

Figure 6.- Continued.

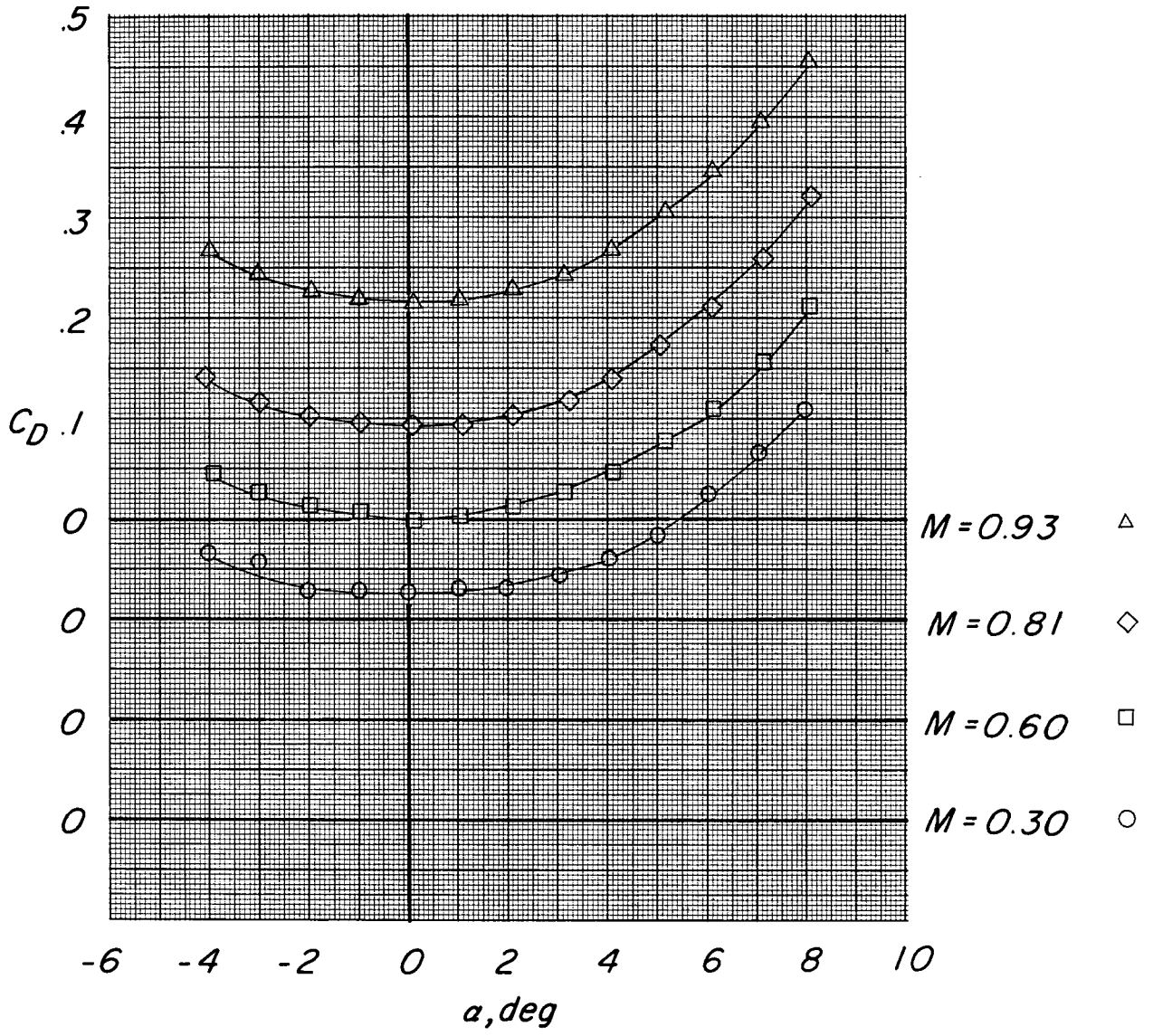

(e) Body with fin 4 arrangement.

Figure 6.- Continued.

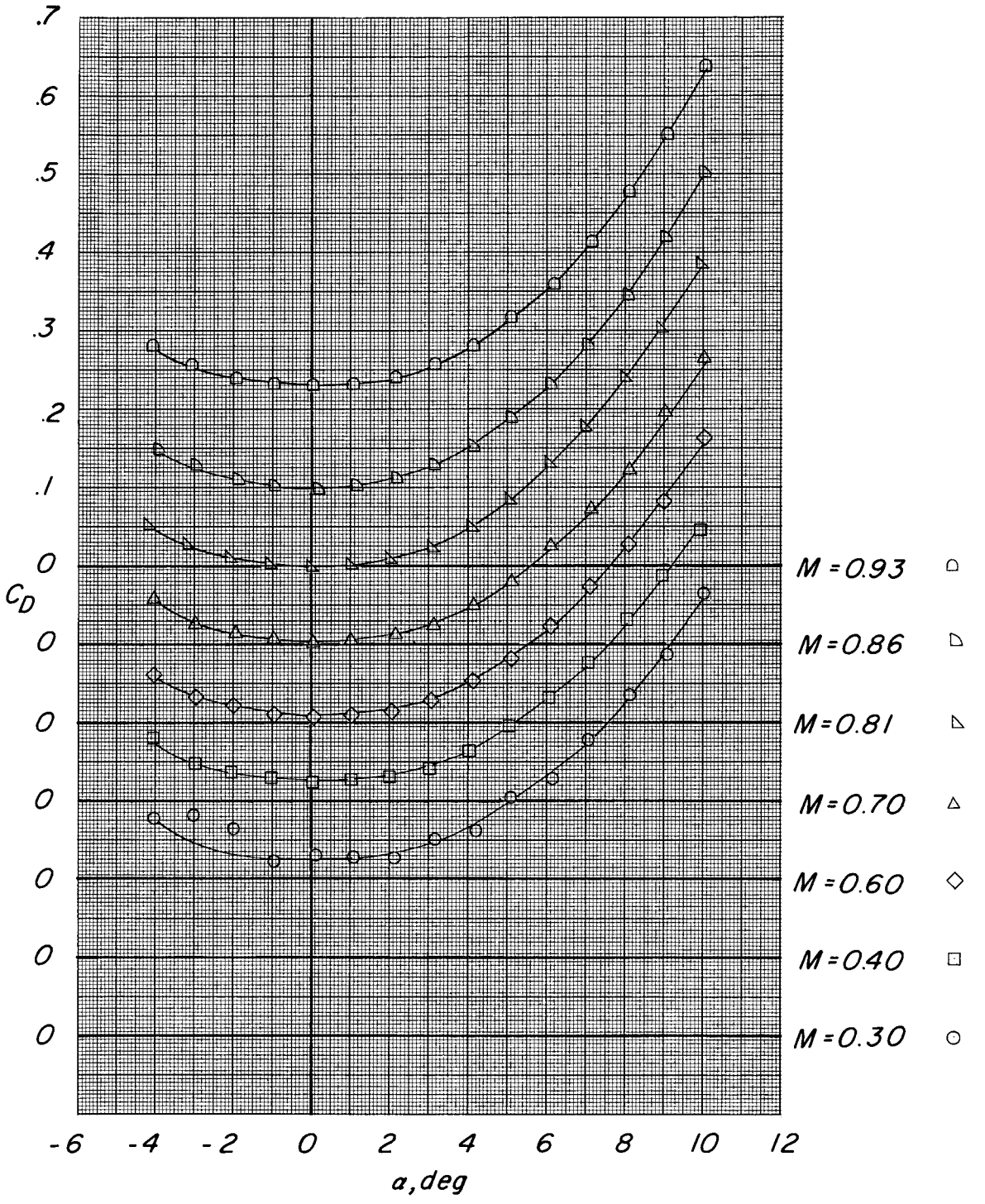

(f) Body with fin 5 arrangement.

Figure 6.- Concluded.

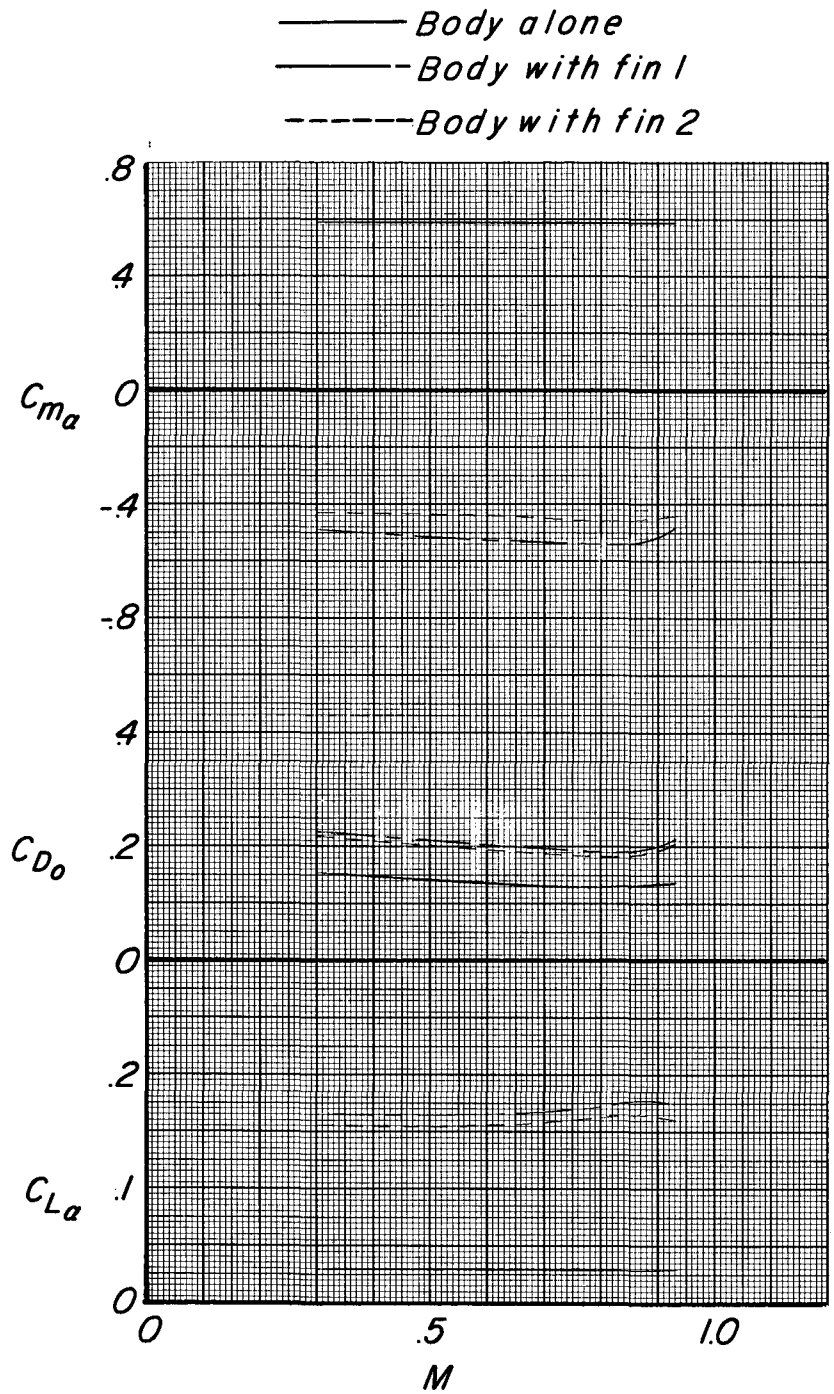

(a) Body alone, body with fin 1, and body with fin 2.

Figure 7.- Effect of various fin arrangements on the longitudinal aerodynamics characteristics of the configuration. $\phi = 0^{o}$.

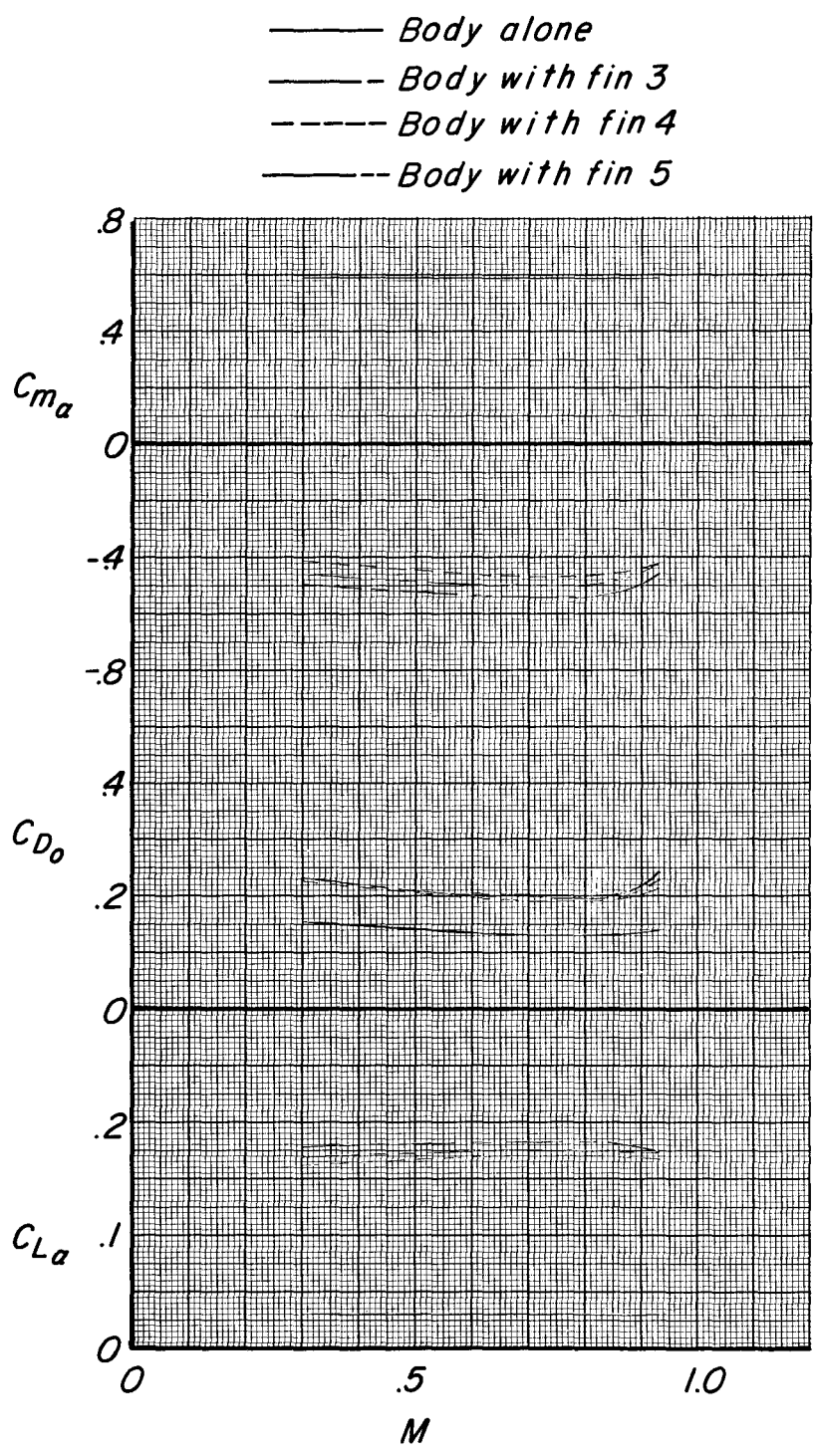

(b) Body alone, body with fin 3, body with fin 4, and body with fin 5.

Figure 7.- Concluded.

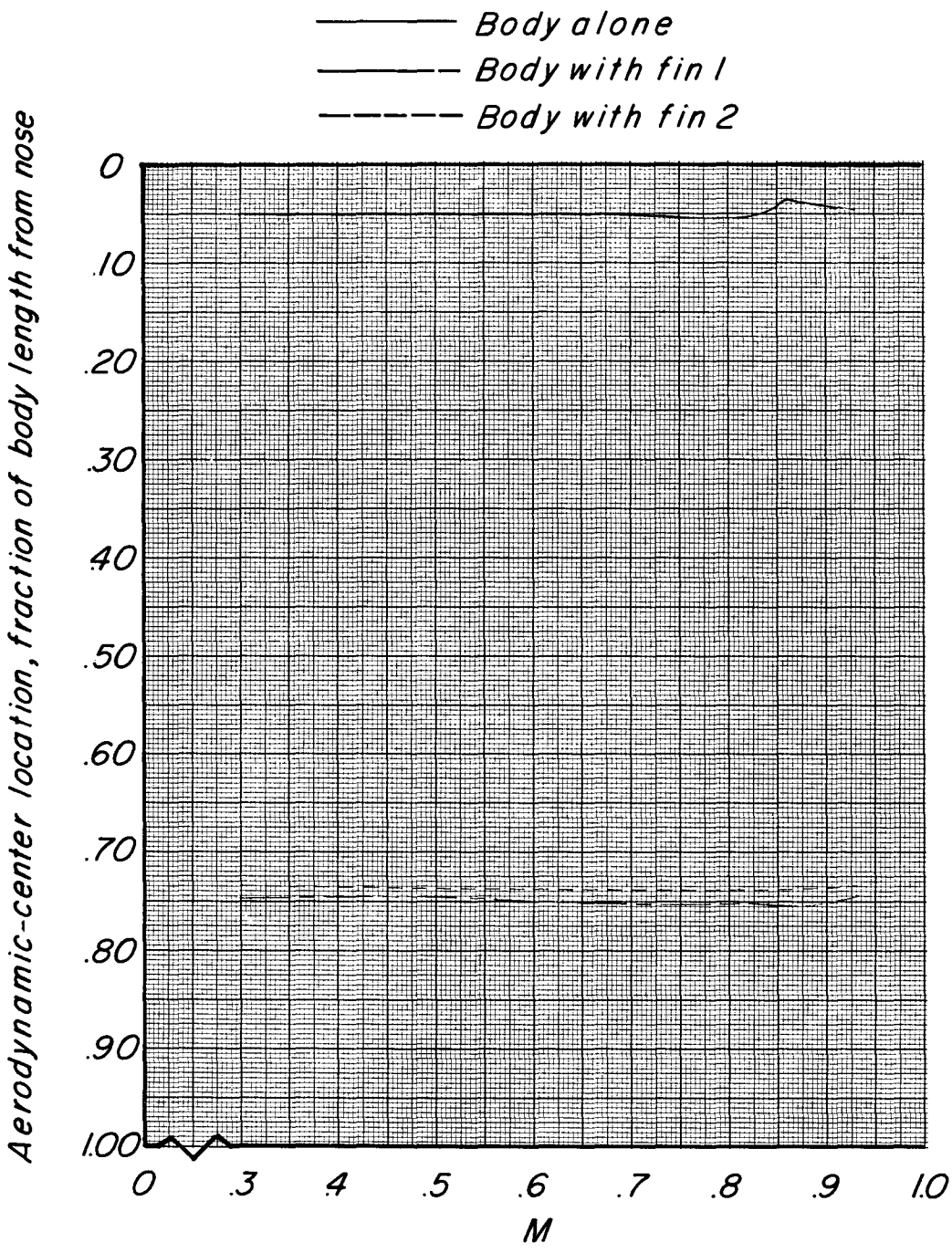

(a) Body alone, body with fin 1, and body with fin 2.

Figure 8.- Aerodynamic-center locations of test configurations. $\phi = 0^{o}$.

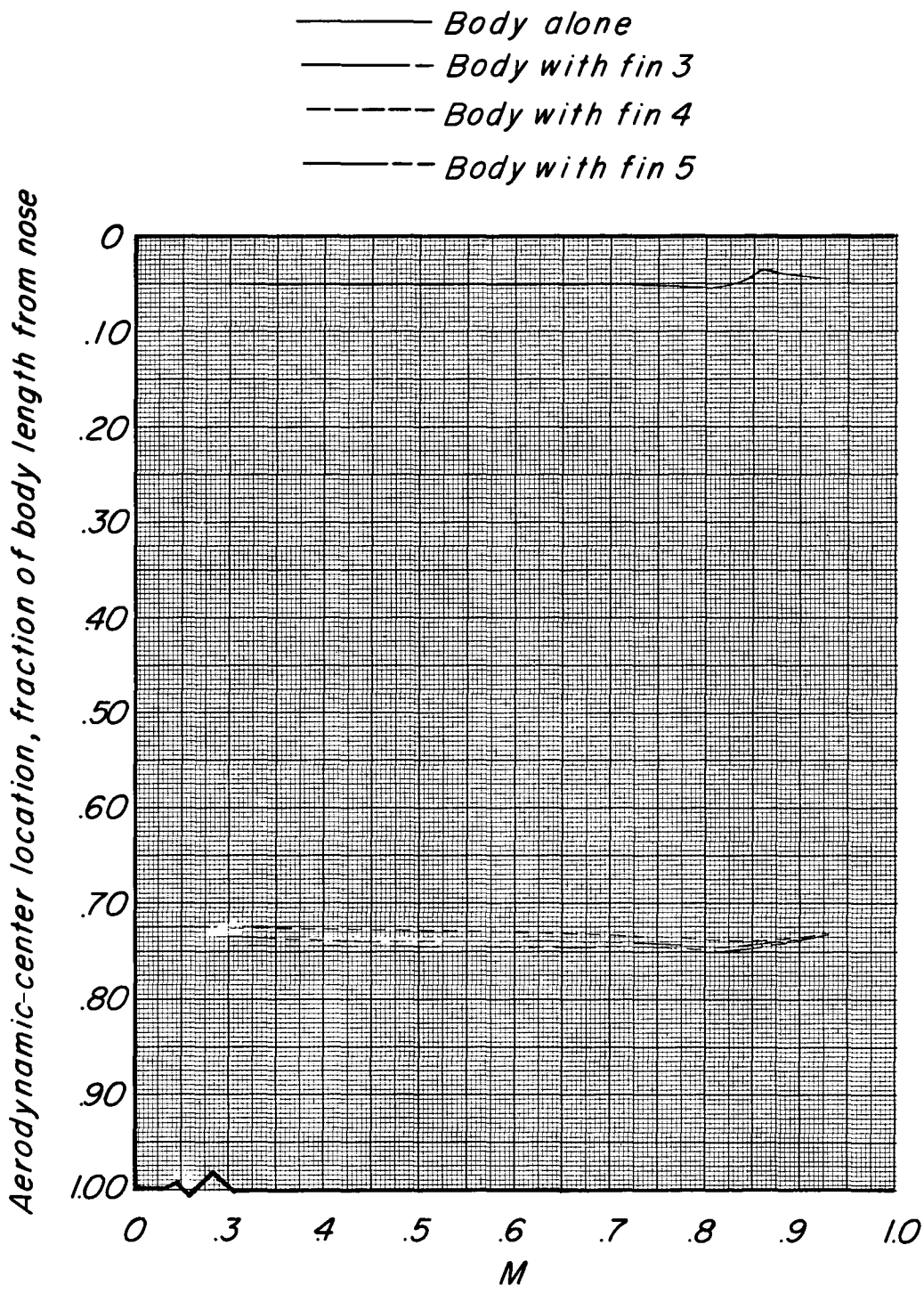

(b) Body alone, body with fin 3, body with fin 4, and body with fin 5.

Figure 8.- Concluded.

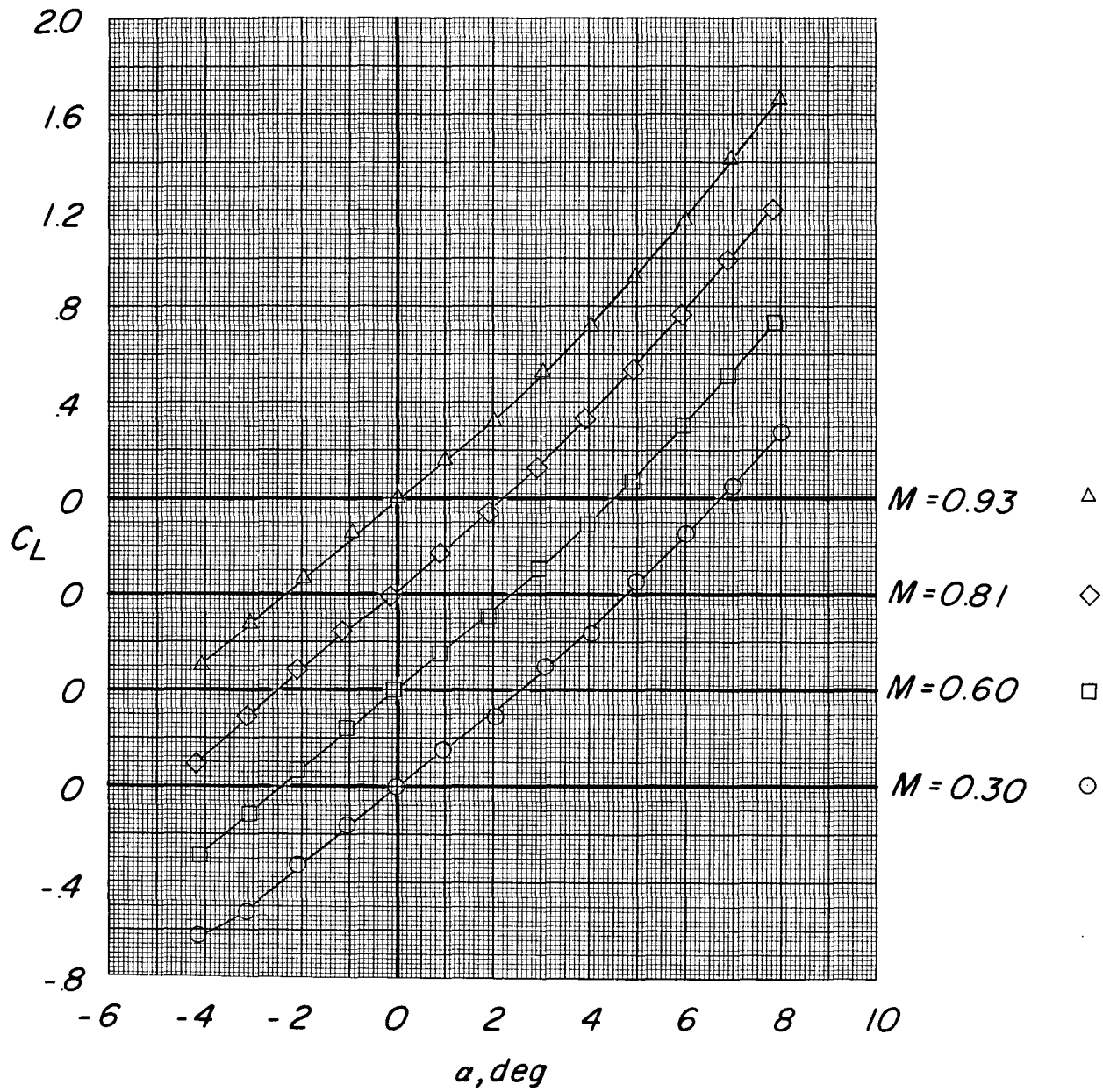

(a) Variation of C_L with α.

Figure 9.- Longitudinal aerodynamic characteristics of configuration with fin 1 arrangement. $\phi = 45^0$.

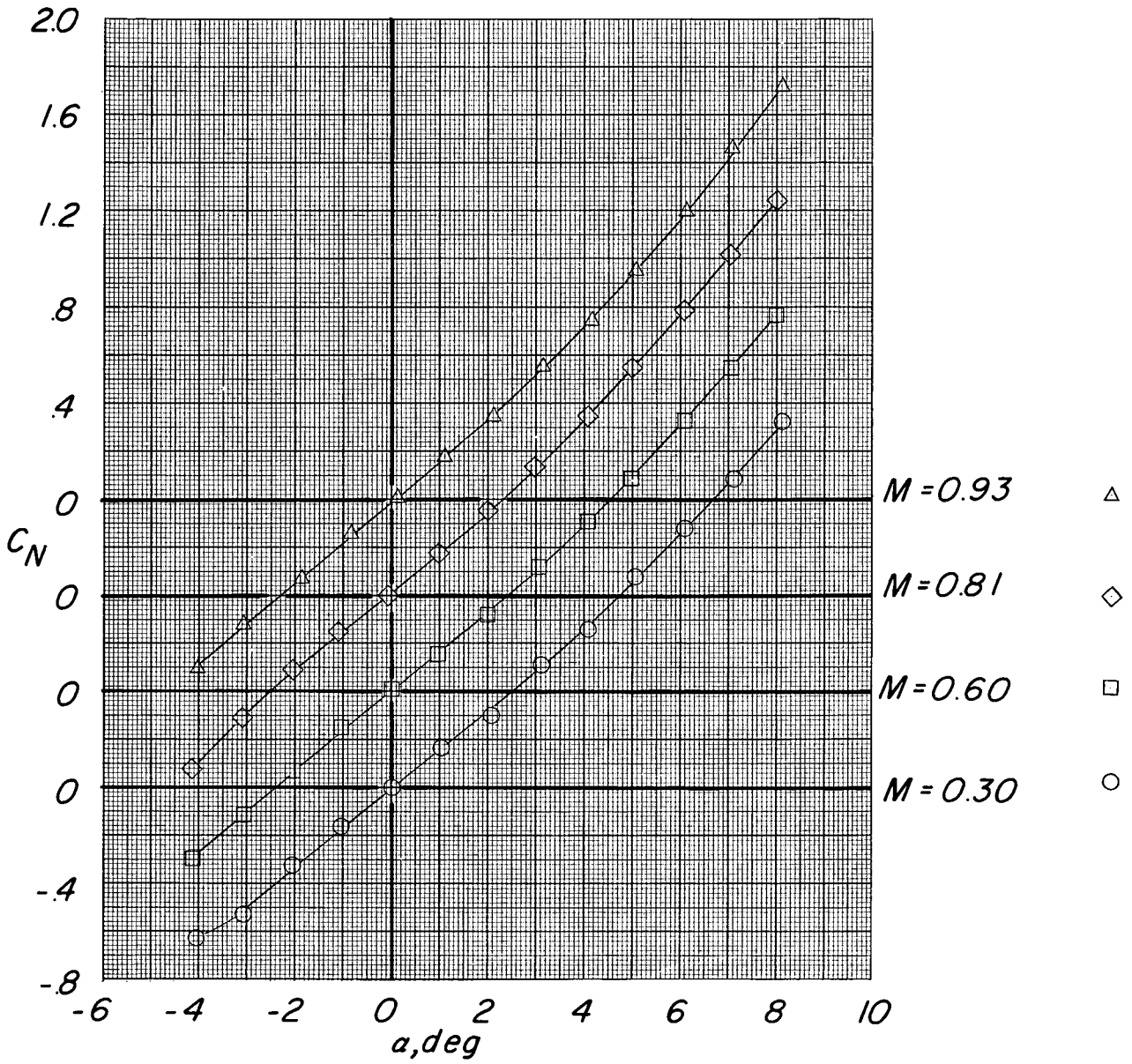

(b) Variation of C_N with α.

Figure 9.- Continued.

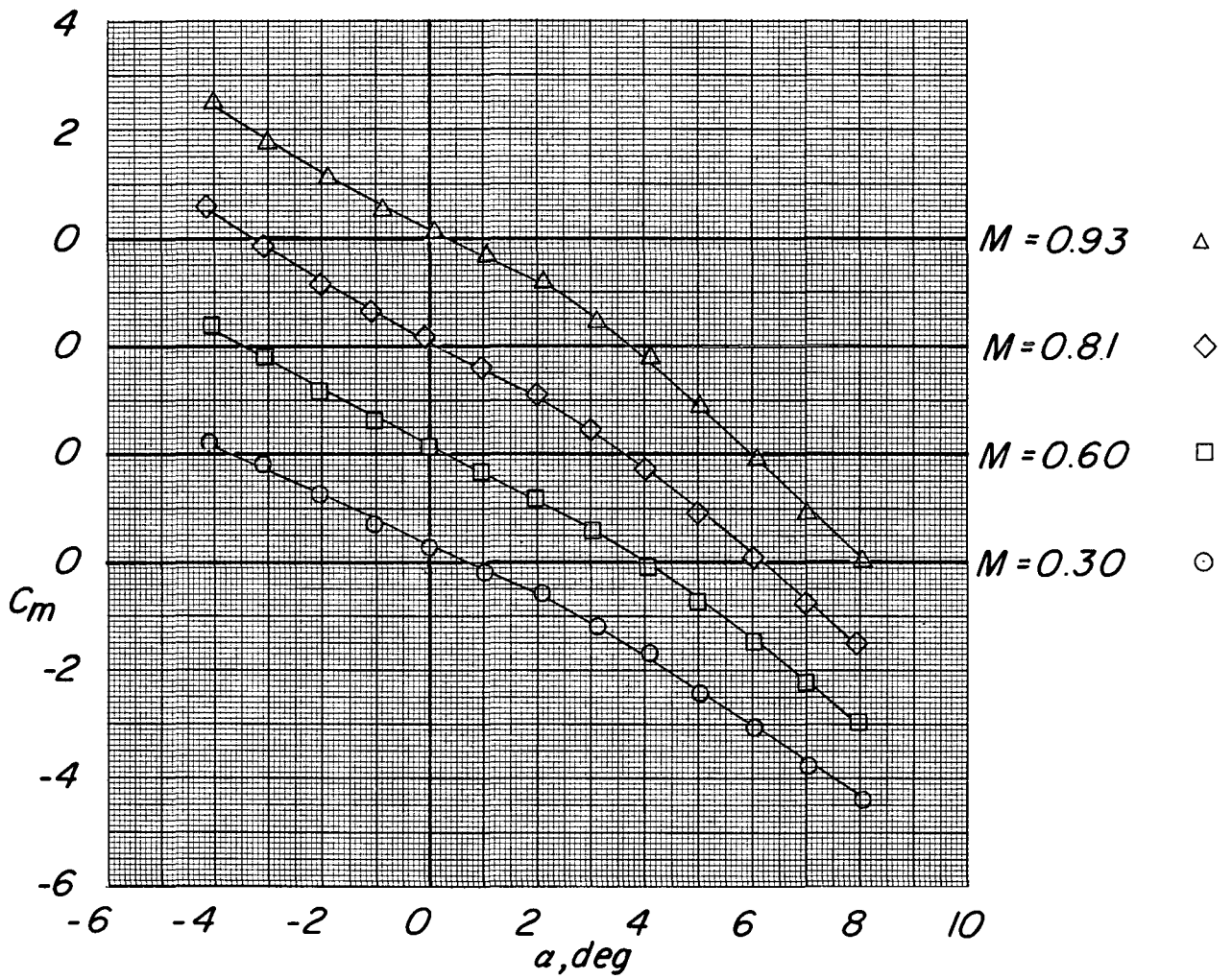

(c) Variation of C_m with α.

Figure 9.- Continued.

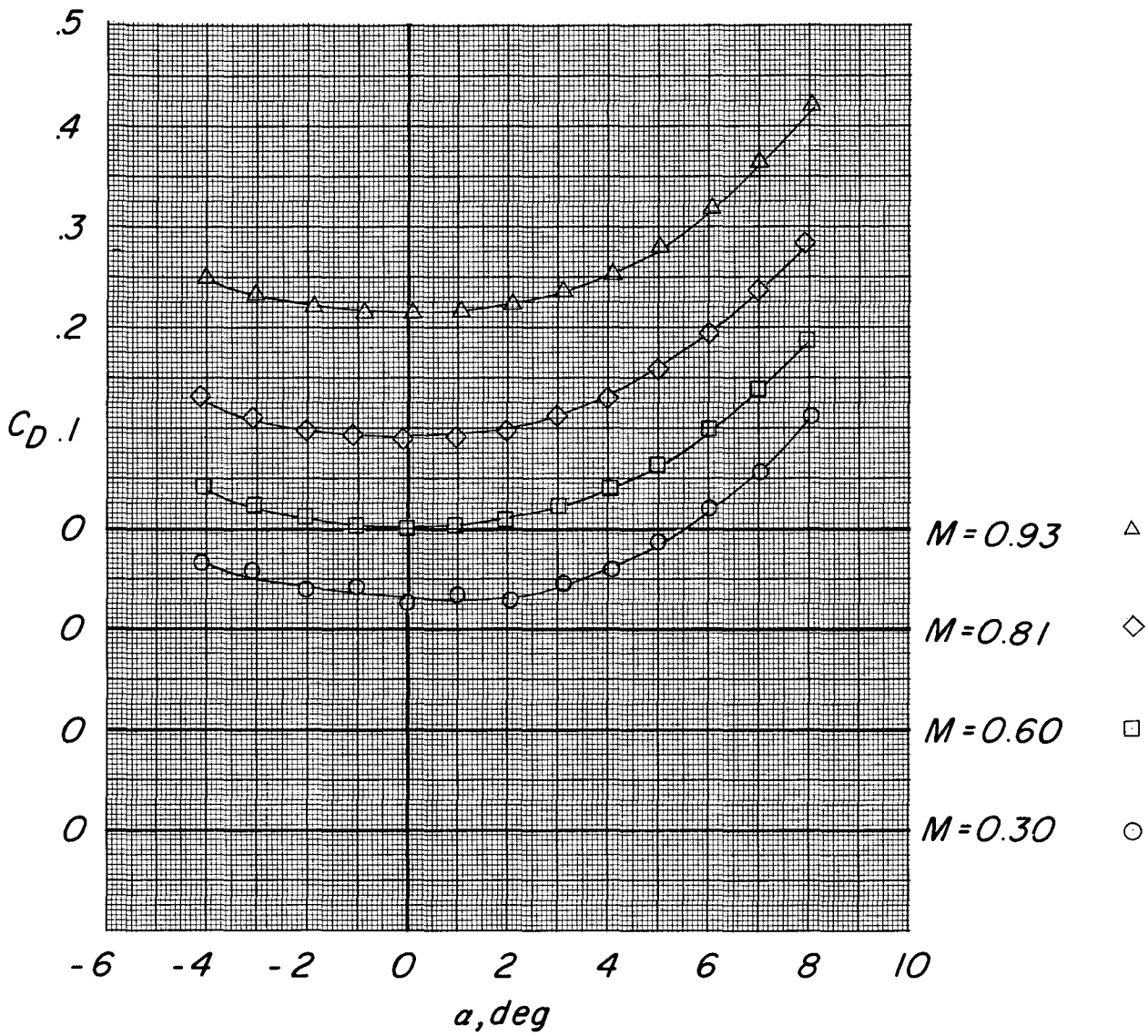

(d) Variation of C_D with α.

Figure 9.- Concluded.

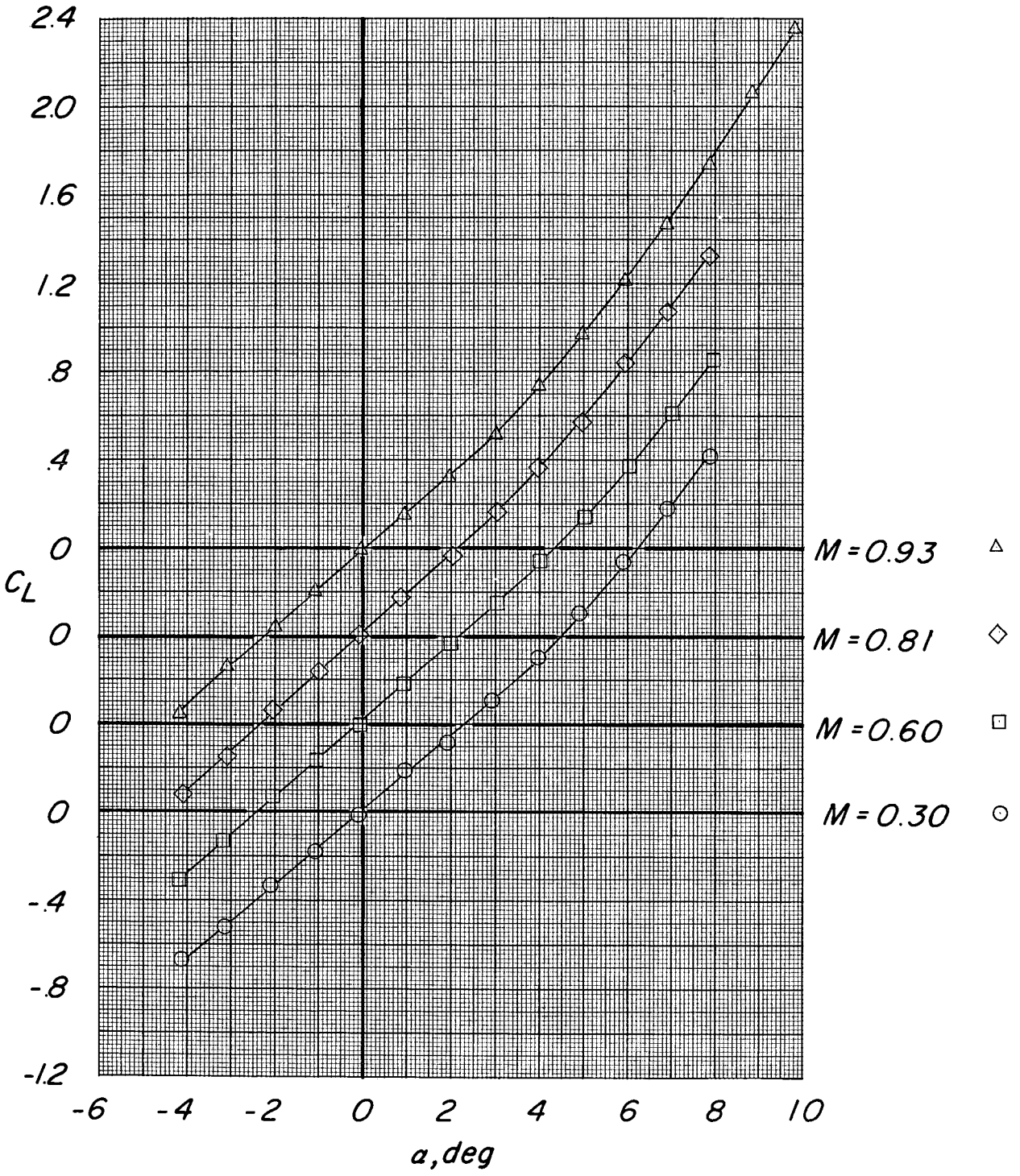

(a) Variation of C_L with α.

Figure 10.- Longitudinal aerodynamic characteristics of configuration with fin 3 arrangement. $\phi = 45^0$.

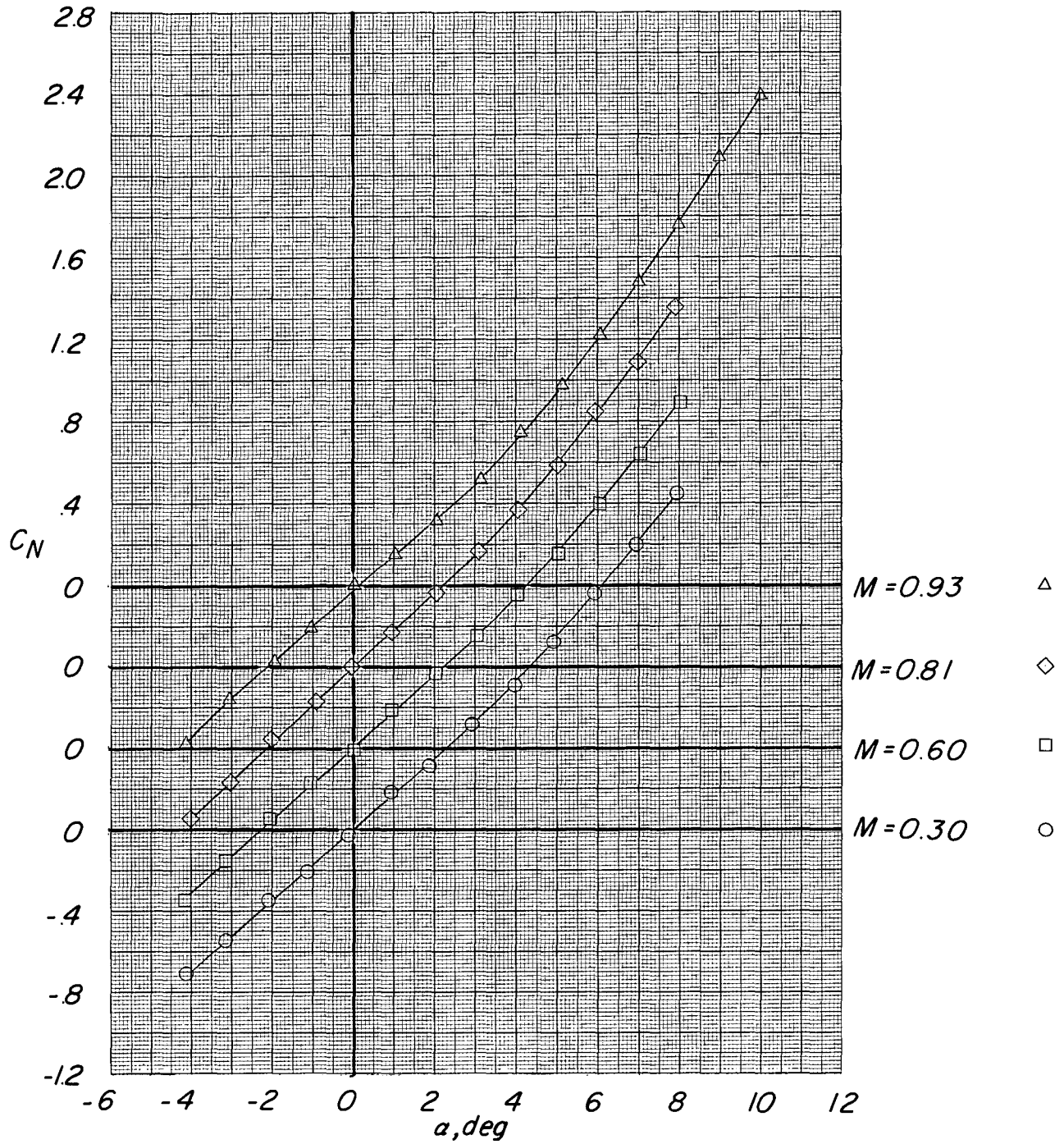

(b) Variation of C_N with α.

Figure 10.- Continued.

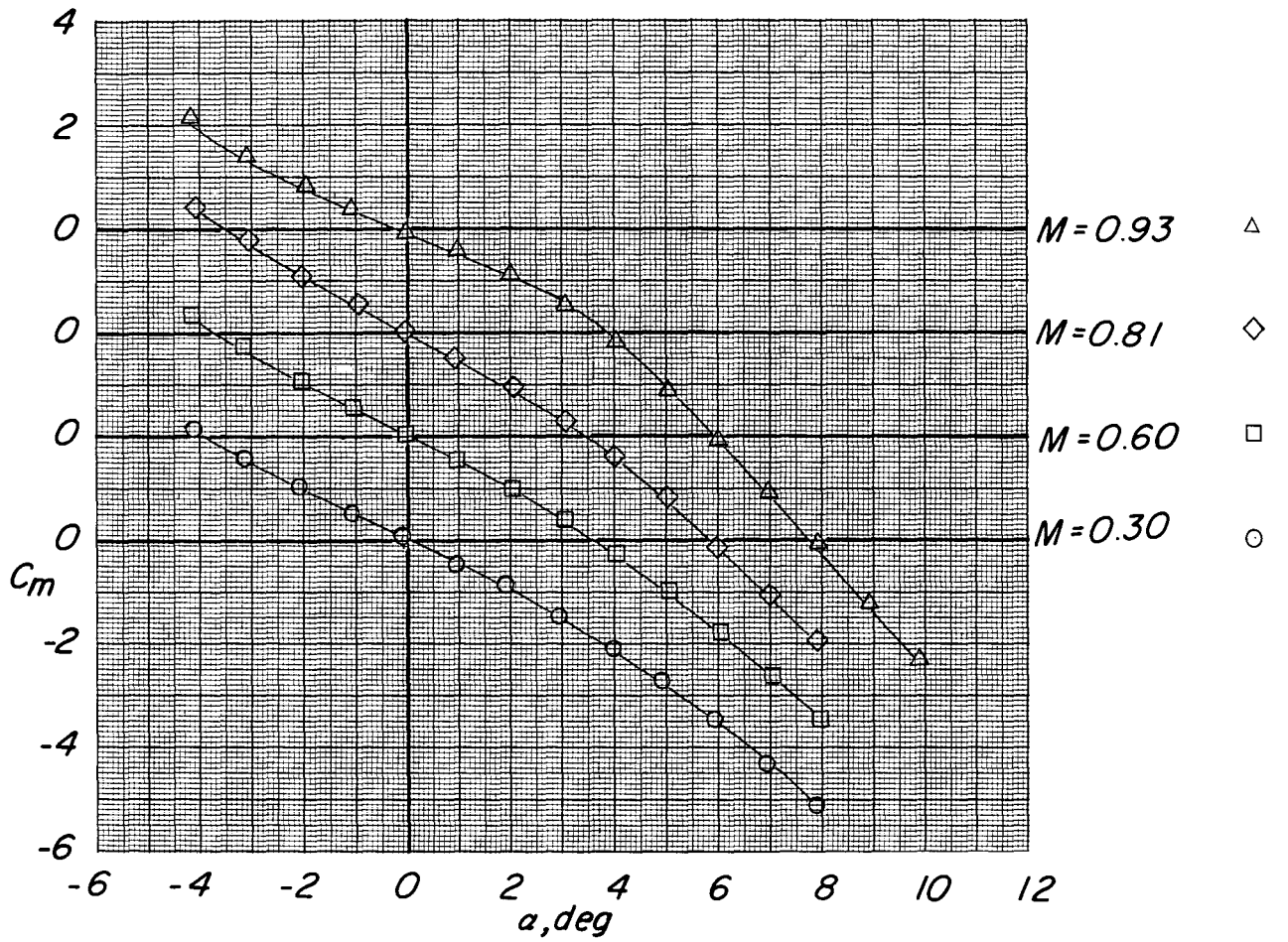

(c) Variation of C_m with α.

Figure 10.- Continued.

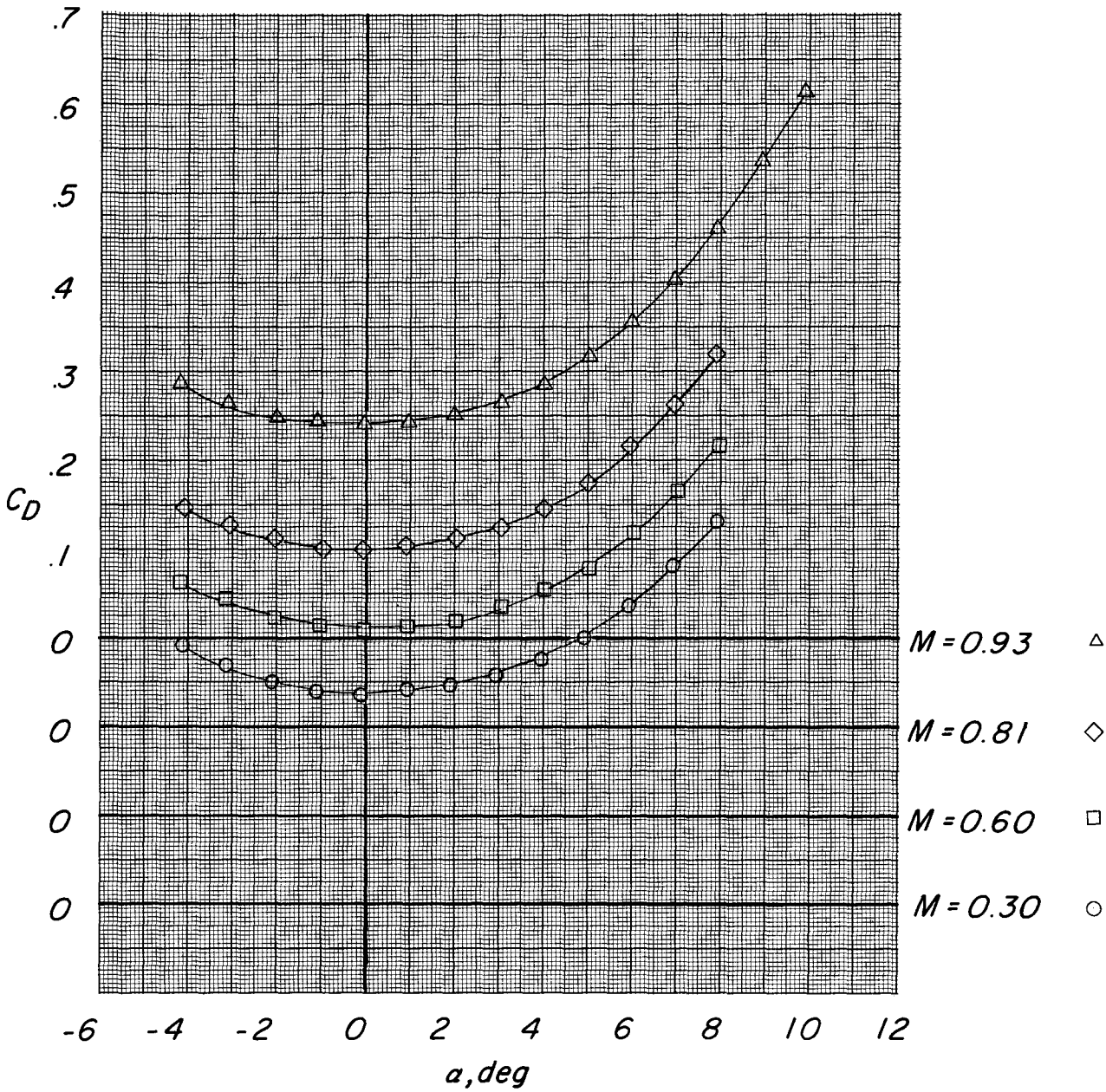

(d) Variation of C_D with α.

Figure 10.- Concluded.

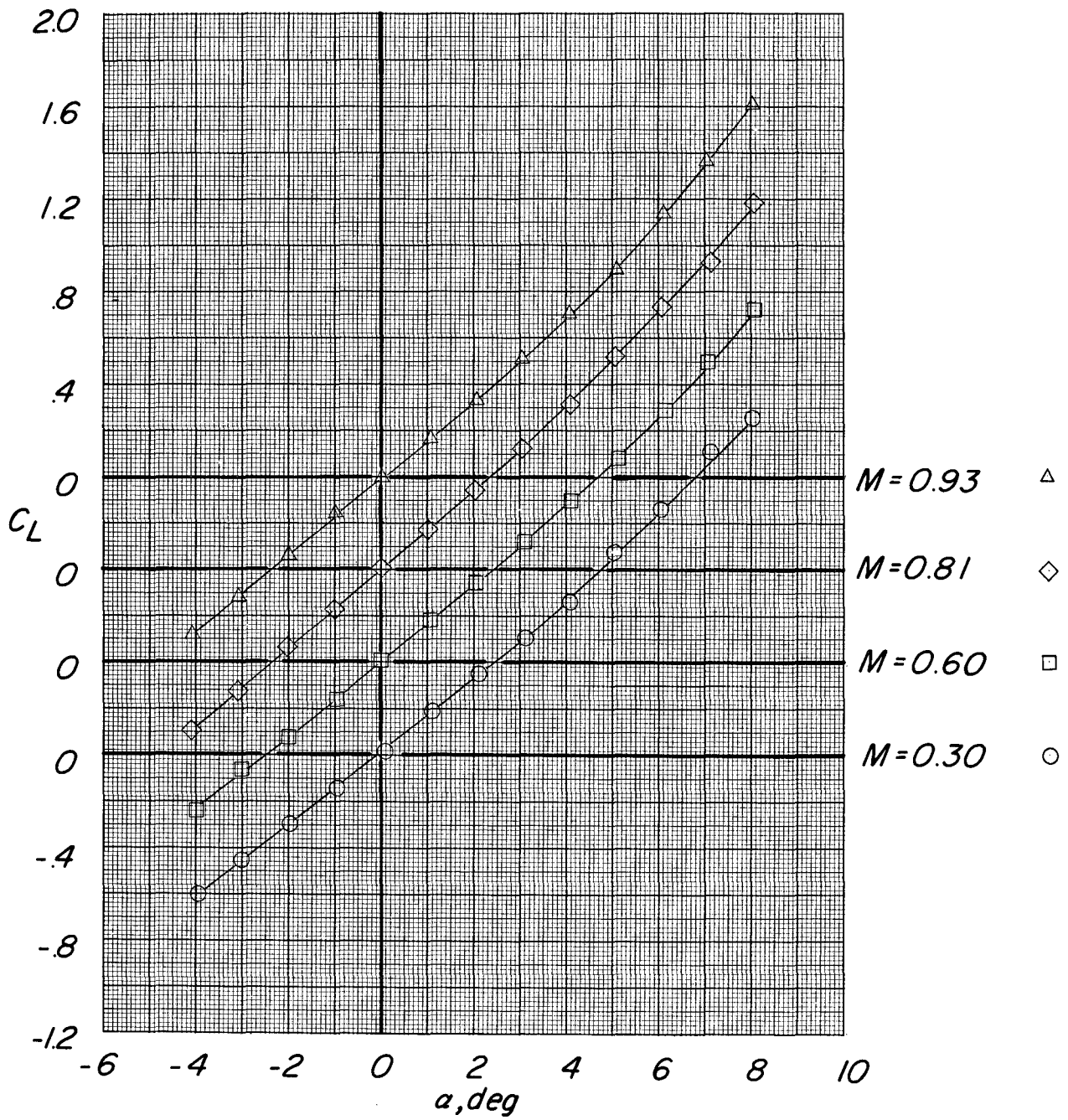

(a) Variation of C_L with α.

Figure 11.- Longitudinal aerodynamic characteristics of configuration with fin 5 arrangement. $\phi = 45^0$.

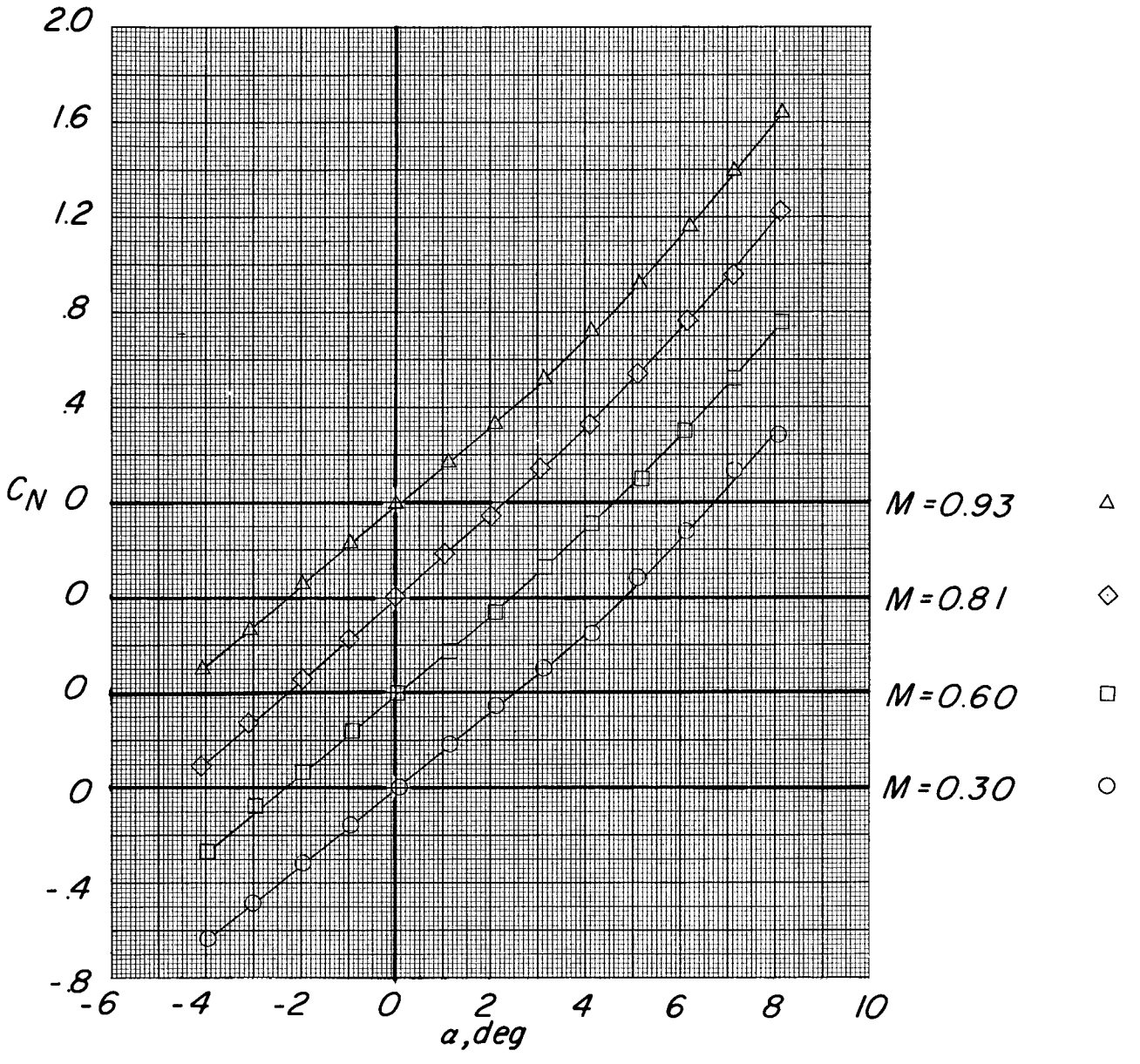

(b) Variation of C_N with α.

Figure 11.- Continued.

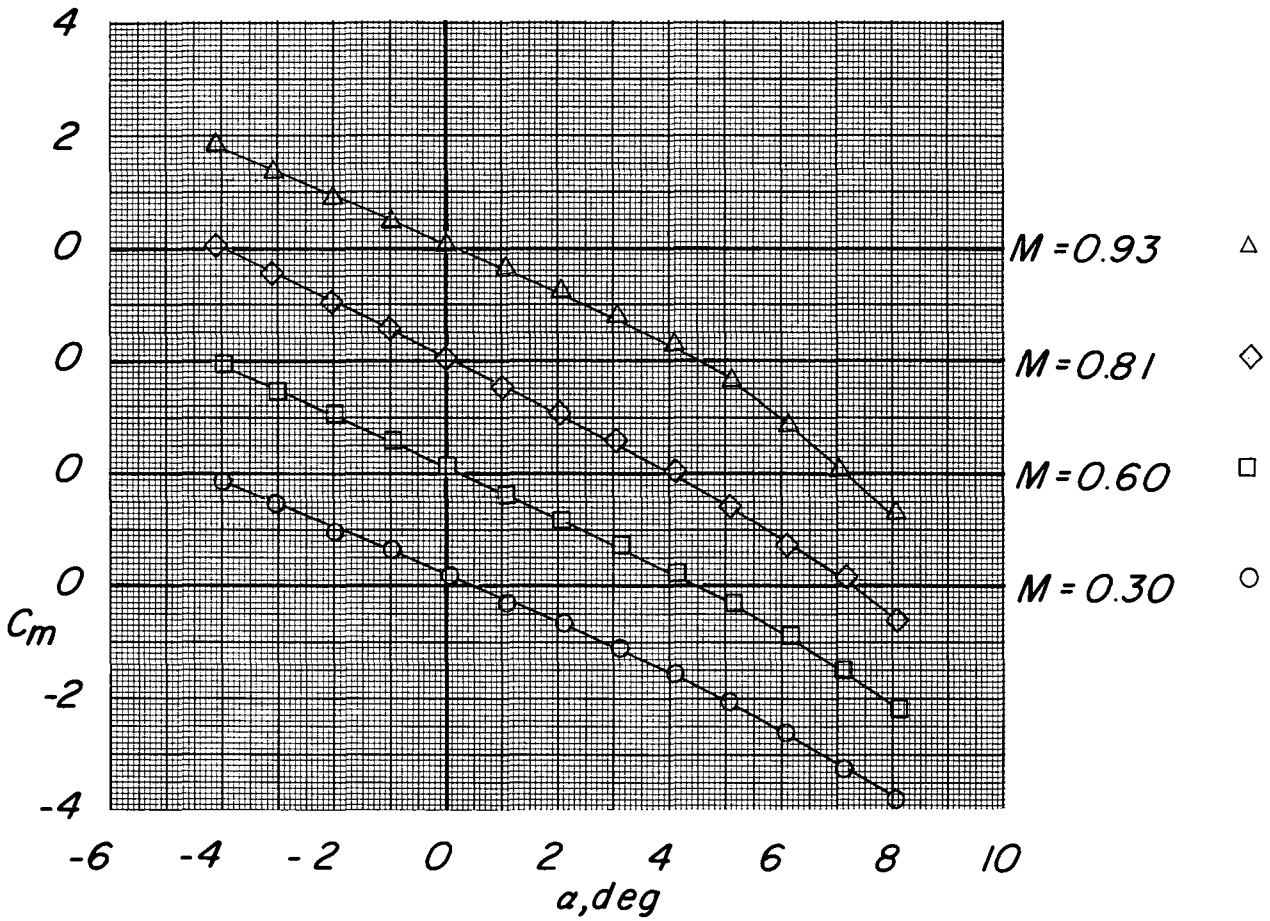

(c) Variation of C_m with α.

Figure 11.- Continued.

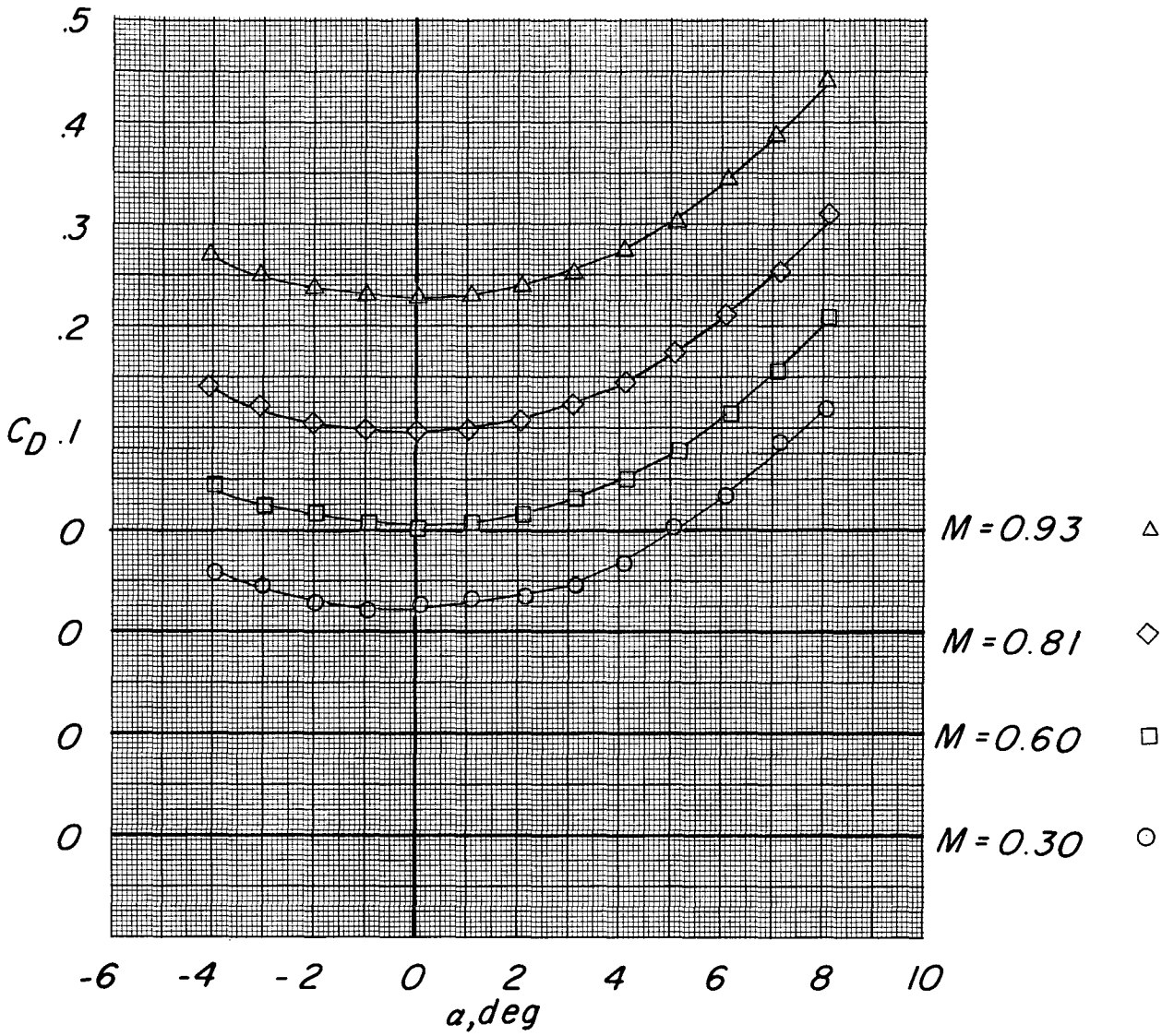

(d) Variation of C_D with α.

Figure 11.- Concluded.

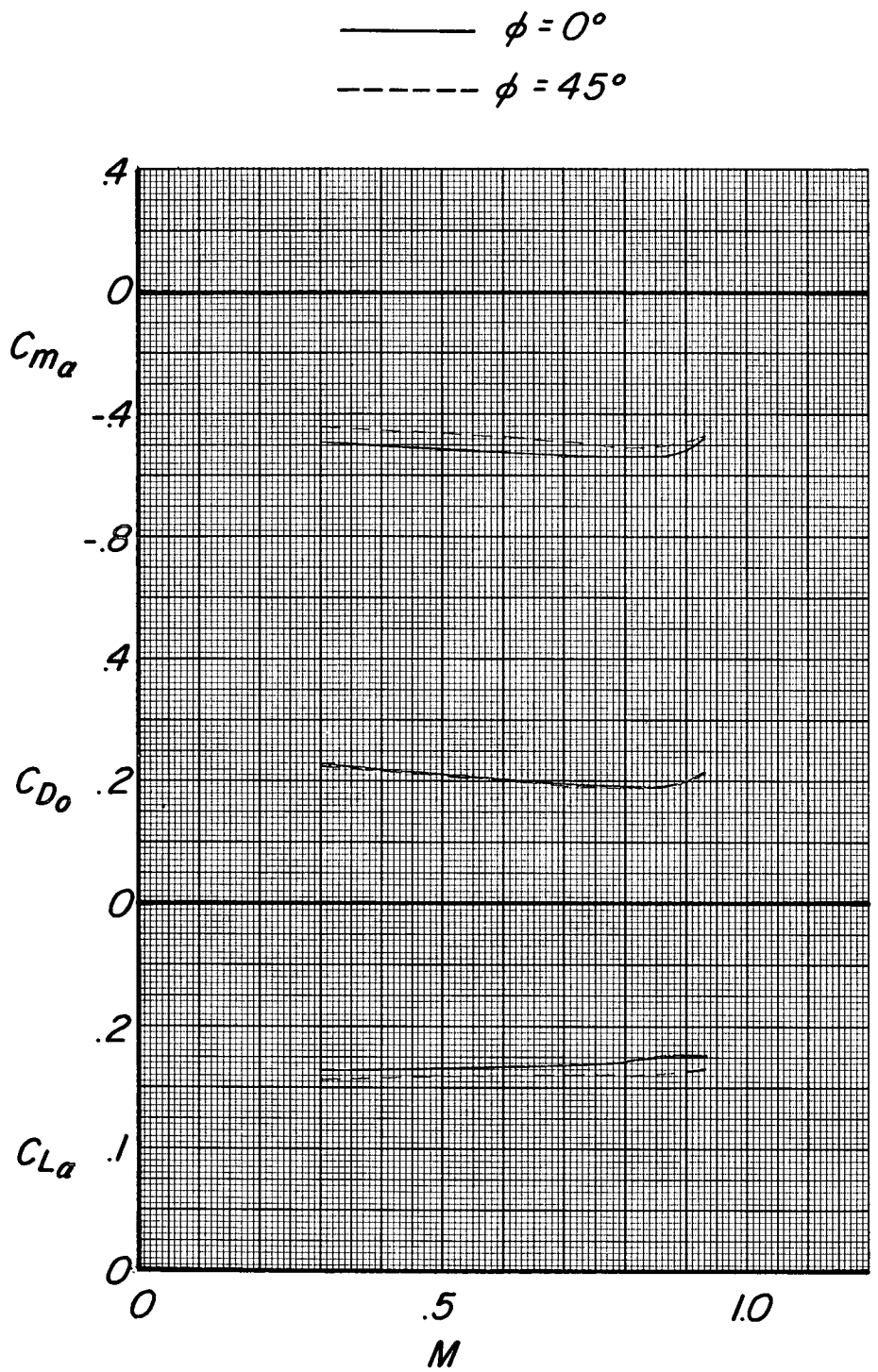

(a) Body with fin 1.

Figure 12.- Effect of roll angle on the longitudinal aerodynamic characteristics of configuration with three different fin arrangements.

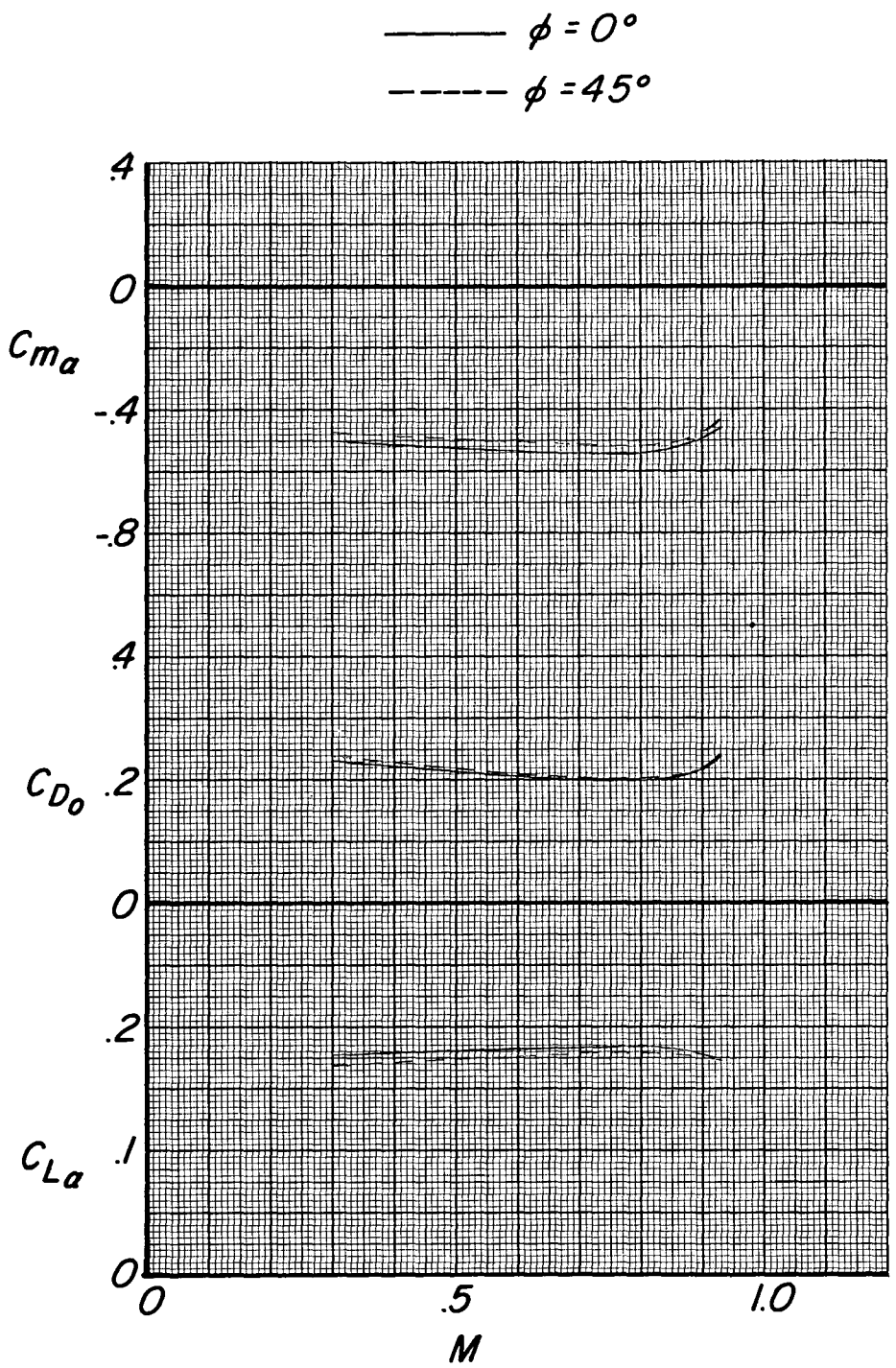

(b) Body with fin 3.

Figure 12.- Continued.

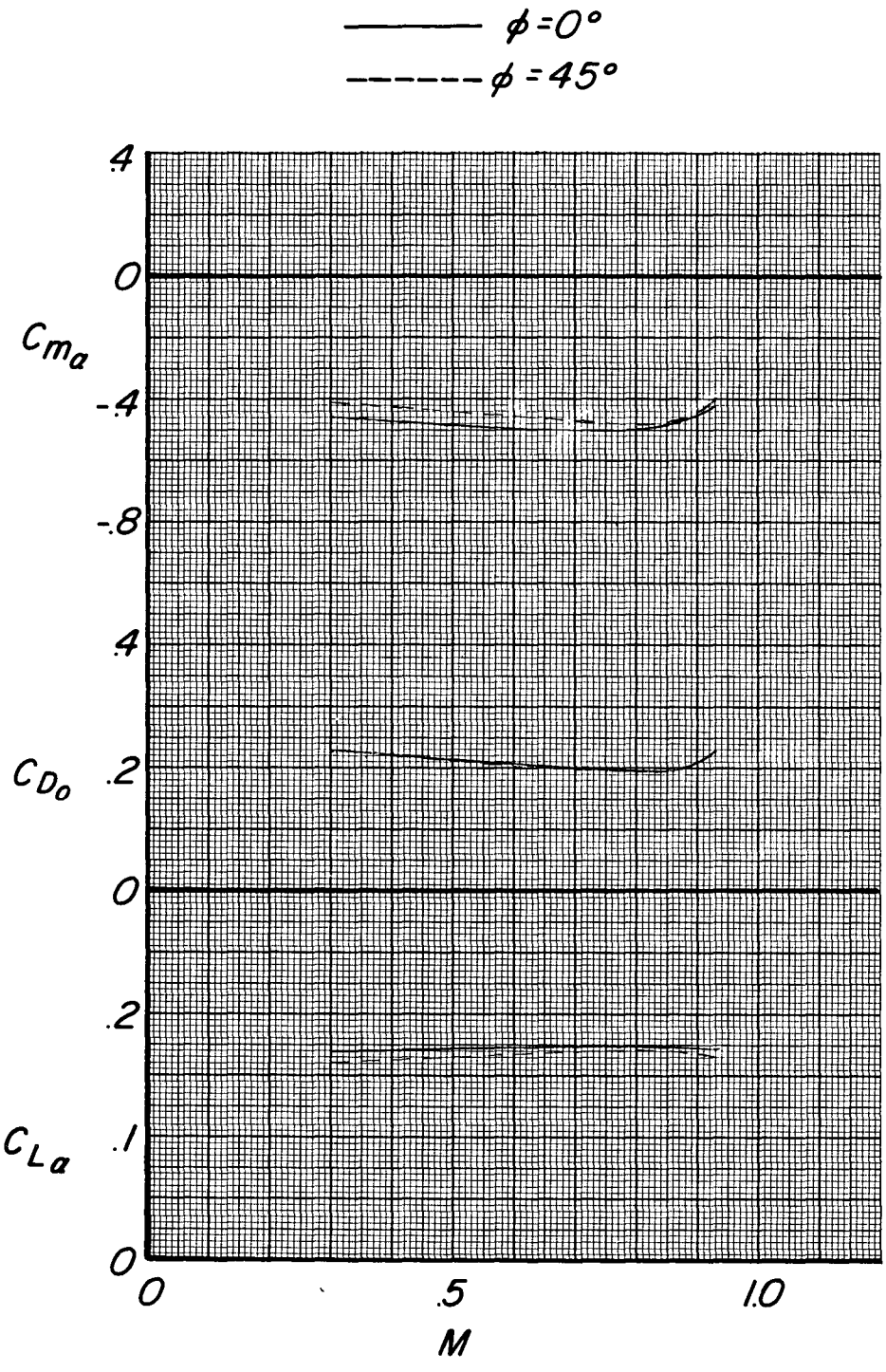

(c) Body with fin 5.

Figure 12.- Concluded.

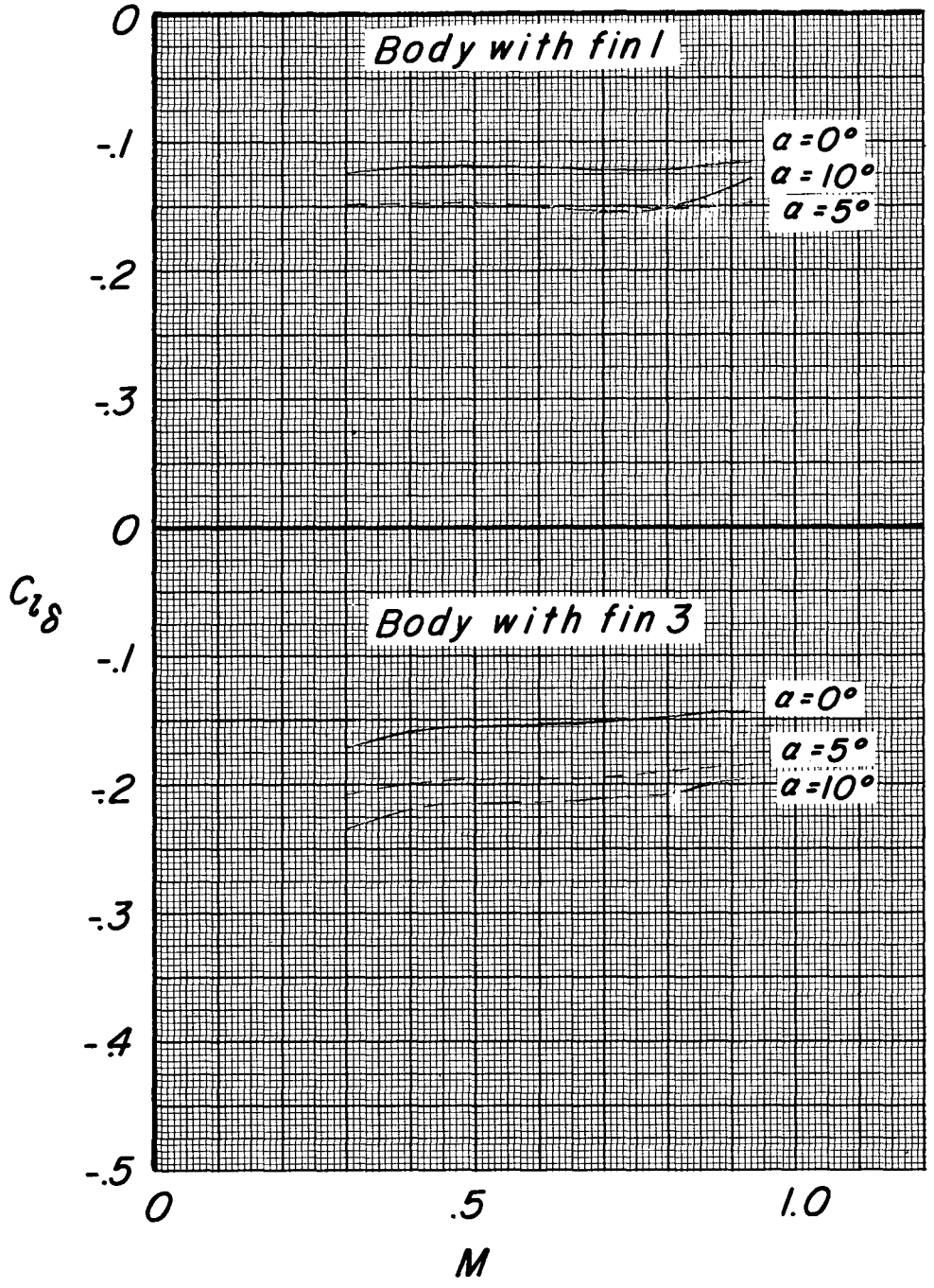

Figure 13.- Variations of roll-effectiveness parameters with Mach number for body with fin 1 arrangement and body with fin 3 arrangement. $\phi = 0^0$.